PHYSICAL REVIEW B **81**, 205310 (2010)

Nature of step-edge barriers for small organic molecules

Joseph E. Goose, Eric L. First, and Paulette Clancy*
School of Chemical and Biomolecular Engineering, Cornell University, Ithaca, New York 14850, USA
(Received 6 January 2010; revised manuscript received 23 February 2010; published 10 May 2010)

A detailed examination of the Ehrlich-Schwöebel barrier that governs transport of molecules over step edges for small organic molecules shows that the nature of this barrier for molecular systems is far richer than has been previously understood. While such barriers for atomic systems can be represented by one numerical value, we show that step-edge energy barriers for molecular systems depend sensitively on the angle of approach to the step edge which, in turn, depends on the ability of the molecule to explore rotational degrees of freedom. Thus a multiplex of barriers can be obtained for edge descent depending on the angle of approach. Studies of seven aromatic molecules (small acenes, C_{60}, rubrene, diindenoperylene, and sexiphenyl) that cover a range of size, shape, and rotational freedom explore how the degree of molecular twisting and bending affects the value of the Ehrlich-Schwöebel barrier on a surface composed of itself ("self"-Schwöebel barriers) and of other organic molecules ("hetero"-Schwöebel barriers). Nonspherical small organic molecules exhibit a strong tendency to "log roll" over step edges at angles around 20° from parallel to the step edge as the lowest-energy descent mechanism. Rigid models of small organic molecules fail to capture conformational flexibility during edge descent, resulting in the production of considerably higher barriers. Intriguingly, while bending and twisting have only a small direct effect on the *magnitude* of the barrier, they play a crucial role on the angle of approach to the step edge which turns out to have a large impact on the barrier height. In addition, we quantify the importance of selecting a sufficiently representative potential model and of employing an appropriately conducted search mechanism. Finally, the broad scope of this study allows us to correlate Schwöebel barriers with the binding energy of the adsorbed molecule to the surface, obviating the need to undertake molecular simulations for molecules not studied here and making possible accurate predictions of self- and hetero-Ehrlich-Schwöebel barriers.

DOI: 10.1103/PhysRevB.81.205310 PACS number(s): 81.15.Aa, 68.43.Jk, 68.55.am

I. INTRODUCTION

The Ehrlich-Schwöebel barrier (hereafter called the Schwöebel barrier) is the energy required for an atom or molecule to descend a monolayer-height step edge *in addition to* that of the conventional surface diffusion barrier as originally proposed by Schwöebel and Ehrlich in separate papers in 1966.[1,2] The existence and size of a Schwöebel barrier plays an important role when considering growth and nucleation of thin films. Large Schwöebel barriers suppress the downward flux of particles between crystalline layers, inhibiting layer-by-layer growth that promotes favored two-dimensional (2D) growth, and instead promote unwanted three-dimensional growth that results when one molecular layer starts growing before the one below it has completed a full monolayer. It is therefore of considerable interest to quantify these barriers in order to understand the morphology of thin-film growth.

Computationally, this barrier has been observed and quantified for monatomic crystals such as copper,[3] aluminum,[4,5] and silicon[6] where the atom's coordination number decreases as it negotiates the step edge, resulting in an increase in potential energy. The inherent symmetry and size of *atomic* systems makes calculation of a Schwöebel barrier tractable, even with fairly sophisticated potential-energy models. In contrast, surprisingly little is known about the nature of Schwöebel barriers for *molecular* systems. Just two previous studies exist that calculate the Schwöebel barrier for organic molecules using molecular simulation techniques: 3,4,9,10-perylene-tetracarboxylic-3,4,9,10-dianhydride (PTCDA) (Ref. 7) and sexiphenyl[8] for which barriers of 80 and 60 kJ/mol, respectively, were reported.

For organic molecules diffusing over step edges, the situation is far more complicated than for atomic systems: The Schwöebel barrier is the *additional* energy required for a particle to diffuse over a step edge compared to the 2D surface diffusional energy. But, for organic molecules, the 2D diffusion pathway on the surface is not easily defined as molecules often do not occupy single sites at any given time.[9] Diffusion in these systems often cannot be characterized as being either "site-site" jumping or continuum random walks and there can be considerable bias in the direction of diffusion. Systems containing small organic molecules are also more complicated due to conformational freedom provided by factors such as the nature and location of their chemical bonds, anisotropic interactions associated with "π stacking," molecular shape, and flexibility. Experimental routes to this energy barrier are indirect; typically, involving scaling models fitted to data collated from atomic force microscopy (AFM) or *in situ* x-ray diffraction, leading to an inferred overall barrier averaged over all possible step types. In contrast, molecular-scale modeling and simulation offers a more direct view of the barrier facing molecules as they approach step edges.

In this paper, we calculate Schwöebel barriers of seven highly aromatic molecules (see Fig. 1) which have significant academic and industrial interest in thin-film applications,[10–12] particularly in the arena of organic semiconductors for flexible displays. The molecules we chose offer some similarities (e.g., degree of aromaticity, chemical

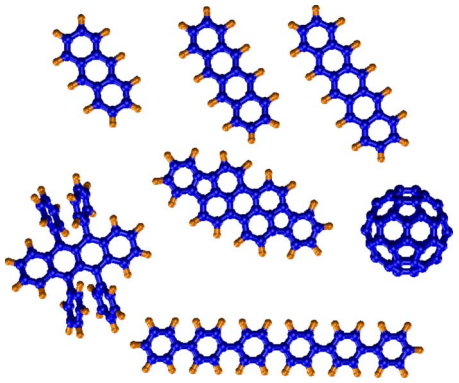

FIG. 1. (Color online) Chemical structure of molecules studied. Clockwise from left: anthracene, tetracene, pentacene, C_{60}, *p*-sexiphenyl, and rubrene with DIP in the center.

structure and overall shape), but they also differ in subtle characteristics that could, we postulated, affect the Schwöebel barrier, such as the presence of single bonds that should increase molecular flexibility. Since there is an almost unlimited array of candidate small organic molecules for thin film growth, we hoped to illuminate some general rules governing the relationship between molecular topology and height of Schwöebel barriers that could lead to an informed choice of candidate molecules for 2D thin-film growth.

A. Software and potentials

For the entirety of this paper the following nomenclature is used, MM3π (Ref. 13) and MM3 (Refs. 14–16) refer to Allinger's MM3(2000) potential, with and without the MP2 π electron correction. AIREBO(t) and AIREBO are the adaptive interactive reactive empirical bond order potentials by Stuart *et al.*,[17] with and without the four-body torsional term.[18] All *ab initio*-based potentials, which were carried out using the GAUSSIAN03 software,[19] are named as in the Gaussian literature. LAMMPS (Refs. 20 and 21) and the TINKER (Ref. 22) molecular modeling packages were used for AIREBO- and MM3-based calculations, respectively.

B. Prior Work: The Schwöebel barrier of sexiphenyl and PTCDA

Both previous molecular simulation studies of Schwöebel barriers (for PTCDA and sexiphenyl) used a nudged elastic band (NEB) method for energy minimization. Such methods require that the number of degrees of freedom is kept low, necessitating that, in both cases, the molecules constituting the step and the underlying substrate were "frozen" (unable to move in response to the interaction with the diffusing admolecule). In addition, the internal degrees of freedom were reduced: In the case of PTCDA, the molecule was held rigid, while—for sexiphenyl—a single parameter was employed to describe the bending of the molecular backbone (keeping all other internal degrees of freedom frozen). A gradient search algorithm was then employed in the remaining rotational and translational degrees of freedom giving rise to a total of 6 and 7 degrees of freedom for PTDCA and

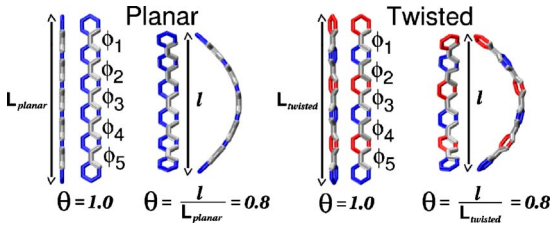

FIG. 2. (Color online) Structure and nomenclature of planar sexiphenyl molecules (ϕ_i=0) and twisted sexiphenyl molecules ($\phi_i \neq 0$).

sexiphenyl, respectively. For PTCDA, where the fused-ring backbone of the molecule is almost certain to remain rigid, and the molecule to remain planar throughout the step-edge descent, we assert that this is a valid assumption.

For sexiphenyl, assumptions of planarity and rigidity are more of a concern. Hlawacek *et al.*[8,23] proposed a mechanism whereby the descending sexiphenyl molecule approached a sexiphenyl (self) step-edge orthogonally (i.e., perpendicular to the edge) and descended by bending (essentially draping itself) continuously over the step edge. In their paper, the molecule was constrained to remain "planar" at all times (i.e., all five torsional angles ϕ_i=0°; see definitions in Fig. 2) leading to a Schwöebel barrier of 60 kJ/mol (0.63 eV) which matched their experimentally determined value to within 10%. Further, the authors claimed that a completely rigid molecule (one not allowed to bend) experienced an energy barrier of 85 kJ/mol (0.9 eV) representing a loss of 70% of the binding energy with the (001) surface. Their results contrasted our experience modeling the Schwöebel barrier of small, rigid organic molecules with a similar structure [i.e., pentacene, anthracene, and diindenoperylene (DIP)] which produced Schwöebel barriers that were considerably smaller than Hlawacek's reported values for sexiphenyl. In addition, our results for relatively rigid molecules showed that the point of their transition over the step edge occurred with the molecular axis almost parallel to the step edge and not orthogonal to the step. This caused us to investigate both the mode of descent and the cause of the larger than expected magnitude of the Schwöebel barrier for sexiphenyl.

II. EHRLICH-SCHWÖEBEL BARRIERS OF SEXIPHENYL MOLECULES

To accurately describe the energy of a molecule descending a step edge, the intermolecular potential must be able to model both (i) the intermolecular interactions between the molecule and the step-edge surfaces and (ii) the internal energy due to the geometrical conformation of the molecule. The model also needs to be computationally efficient enough to allow sufficient sampling of step-edge descent both in terms of time and system size (we typically use 2000–3000 atoms to describe the step and underlying substrate). We started by examining how well certain potentials were able to describe the conformational phase space of the isolated molecule, specifically its propensity to twist and bend.

A. Molecular structure of sexiphenyl

Initially, interest centered on the effect of free rotation of benzene rings around C—C bonds in the sexiphenyl mol-

ecule as a possible cause of the high barrier reported by Hlawacek *et al.* In that regard, there have been a number of papers on the degree of planarity and structure of sexiphenyl[24] and similar molecules.[25–32] However, these issues are still far from resolved, even for the relatively simple isolated biphenyl molecule. For further discussion and calculation of isolated single torsional potentials of biphenyl and sexiphenyl see Appendix A.

1. Molecular-structure notation

We first define some notation to describe the conformation of the molecules (see Fig. 2). Molecular bending is described by a normalized molecular length, $\theta = l/L$, where l is the distance between the terminal carbon atoms and L is the length at the minimum energy structure. We use the term planar for molecules where all torsional angles across the C—C single bond are zero, i.e., $\phi_i = 0°$. We use the term "twisted" for molecules in which all the torsional angles are $\neq 0°$. The torsional potential around one C—C single bond is described by ϕ_{min}.

2. Geometry optimization on the sexiphenyl molecule

a. Unbent molecules. We first undertook calculations on isolated unbent molecules using a variety of models ranging from basic Hartree-Fock (HF) and MP2-corrected methods to density-functional-theory (DFT) methods, and including the fully atomistic AIREBO (Ref. 17) and MM3 models. We performed unrestrained geometry optimizations on the molecule to probe the extent of twisting and constrained $\phi_i = 0$ to examine planar molecules. Molecular lengths of planar molecules were very similar irrespective of the potential used. In contrast, AIREBO models slightly underpredicted the length of the twisted molecules in comparison to others presumably because the larger $\phi_{min(i)}$ reduced steric hindrance between neighboring phenyl rings. All models predicted a twisted molecular energy minimum, rather than planar, with the exception of the MM3. Twisted molecular minima adopted a conformation where the torsional angle between neighboring benzene rings alternated between positive and negative offsets along the molecular axis designated as (+−+−+). From Table I, predicted torsional angles of all tested models, with the exception of AIREBO(t), fall into the range of 30°–50° which encompasses all previous calculations and experimental values for *para*-phenylene oligomers up to *p*-heptaphenyl. The same general behavior is seen for sexiphenyl, as previously observed for biphenyl,[27] in that HF and MP2 (and both AIREBO) overpredict the twist barrier $\Delta E_{p\text{-}t}$ (ΔE_0) and in that DFT methods slightly underpredict torsional angles. We report only terminal torsional angles ($\phi_{1,5}$) since variation along the molecule is small.

b. Bent molecules. Flexibility of the sexiphenyl molecule around its single C—C bonds leads to expectations that it could bend to some degree as it descends the step edge, as shown in the Hlawacek paper. The following discussion concerns geometry optimizations on sexiphenyl molecules under varying degrees of bend starting from both planar and twisted configurations achieved by constraining the distance between terminal carbon atoms. For planar molecules, it was sometimes necessary to constrain all five ϕ_i in cases where, otherwise, the optimizations led to the spontaneous formation of the twisted minimum-energy conformation. Figure 3(a) shows *all* potential models tested agree that the relationship between bending energy (ΔE_{bend}) of planar molecules and reduction in normalized molecular length (1-θ) is roughly linear. A reduction of 20% in the distance between terminal carbons results in a rise of ≈5 kJ/mol. MM3π is a significant improvement over potential and almost indistinguishable from the *ab initio* and DFT calculations which are many orders of magnitude slower in CPU time. The effect of bending on the energy of twisted molecules in minimum energy, alternating twist (+−+−+), conformation showed the same qualitative results as for planar molecules; see Fig. 3(b). Note that all energies are shifted by $\Delta E_{p\text{-}t}$ over the range of θ, i.e., difference in energy between planar and twisted configurations of the sexiphenyl molecule. Thus, results in Figs. 3(a) and 3(b) are each shown relative to their own energy "baseline." Again, all *ab initio* and DFT models (with the exception of Hartree-Fock) and MM3π are in good agreement. Twisted molecules exhibited an increase in en-

TABLE I. Properties of unbent molecules: distance between terminal carbon atoms for planar (L_{planar}) and twisted ($L_{twisted}$) sexiphenyl molecules, energy difference between twisted, and planar minima ($\Delta E_{p\text{-}t}$), *cis*-torsion angle across the terminal C—C single bond ($\phi_{min(1,5)}$).

Model	L_{planar} (Å)	$L_{twisted}$ (Å)	$\Delta E_{p\text{-}t}$ (kJ/mol)	$\phi_{min(1,5)}$ (°)
HF/6–31G(d)	24.62	24.33	68.8	44.6
B3LYP/6–31G(d,p)	24.65	24.45	36.3	37.2
PBEPBE/6–31G(d,p)	24.72	24.53	31.9	35.7
MP2/6–31G(d,p)	24.60	24.32	73.1	42.0
MM3π	24.65	24.43	30.0	35.3
MM3	23.50	N/A	N/A	N/A
AIREBO(t)	24.44	23.88	250.9	66.3
AIREBO	24.44	23.95	131.2	41.0

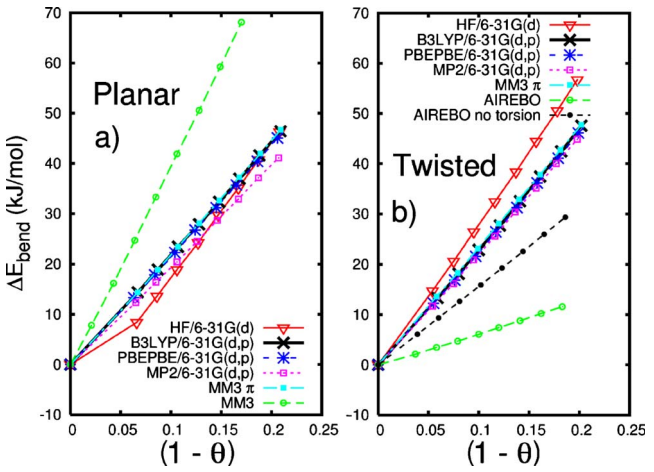

FIG. 3. (Color online) The effect of bending on the energy of isolated (a) planar and (b) twisted molecules.

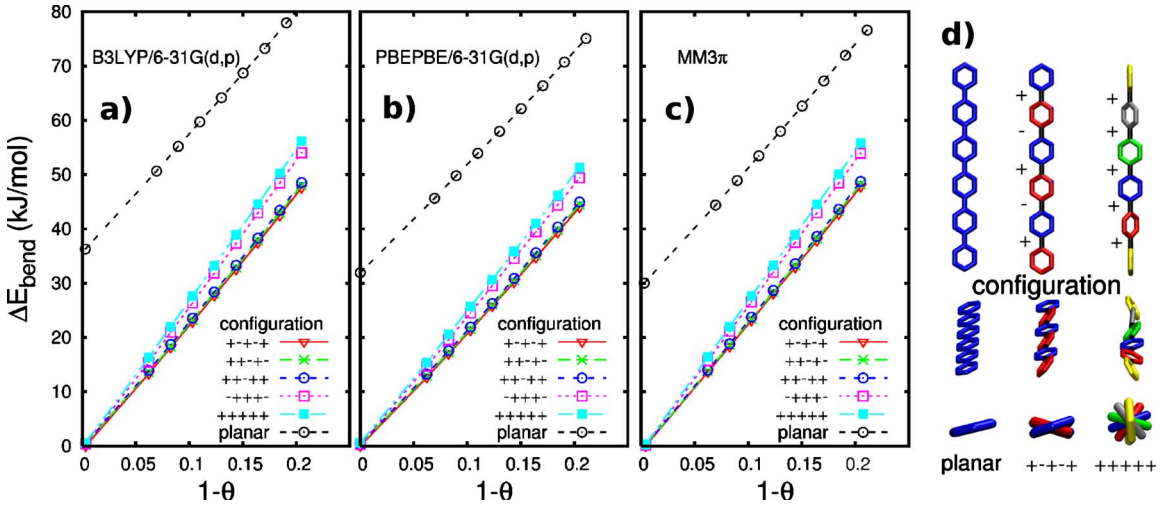

FIG. 4. (Color online) Bending energies for five different twisted configurations and planar molecules relative to the global minimum (+−+−+) twisted straight molecule energy. (a) PBEPBE/6–31G(d,p), (b) B3LYP/6–31G(d,p), (c) MM3π, and (d) Configuration nomenclature for twisted molecules

ergy of roughly 50 kJ/mol for a reduction in end-to-end distance of 20%. The AIREBO(t) potential was a noticeable outlier, predicting bending of the molecule was not as energetically unfavorable. By removing the torsional term of the AIREBO potential,[18] the cost of bending was increased; however, the barrier was still significantly less than all other methods and suggests this model is not a good choice for sexiphenyl.

3. Alternate configurations of twisted molecules

We use a +− notation, see Fig. 4, to describe the many possible neighboring twists along the sexiphenyl molecule. Preliminary calculations predicted the unbent twisted conformation was a global minimum, irrespective of the way molecules were twisted; the length of molecules was also constant for any given potential. However, when twisted molecules were bent, small variations in energy arose due to conformational differences along the molecule. The two extremes were the alternating twist (+−+−+) and the helical twist (+++++), as shown in Fig. 4(d). In Fig. 4, we plot ΔE_{bend} for five different twisted configurations and for the planar molecules as we increase the degree of bending for the MM3π, PBEPBE, and B3LYP models. Agreement among them is remarkable considering the difference in model complexity (and hence differences in the CPU time taken).

Overall, the ability of MM3π to reproduce the DFT results is very encouraging and leaves us confident that we can use this model to examine the Schwöebel barrier of sexiphenyl more accurately than previous efforts. The torsional potential is shallow around ϕ_{min} so the effect of underpredicting the angle slightly will not have a large effect on the system energies. These results suggest that the intramolecular forces are well described by MM3π.

B. Intermolecular interactions

Intermolecular forces in the MM3(π) potentials are described by a pairwise additive, modified Buckingham exp(−6) potential with an additional electrostatic contribution from C—H dipole moments. The intermolecular potential was parameterized against a large data set of heat of sublimation and molecular crystal parameters for both aliphatic and aromatic molecules. Importantly the data set included both benzene and biphenyl molecular crystals—the building blocks of our molecule set. We are confident of the applicability of such a model because intermolecular potentials of this kind [including the similar DREIDING (Ref. 33) potential which implements a 12–6 instead of exp(−6) van der Waals contribution] have been used to examine complex crystal structures of several organic molecules such as pentacene, tetracene, perylene, and 1,2-dimethoxyethane.[34–37] For the rest of this paper, we concentrate on applying the MM3π potential to model the molecules considered here.

C. Descent of a sexiphenyl molecule over a step edge

We now turn our attention to simulating the descent of an MM3π-modeled sexiphenyl molecule over a step edge composed of sexiphenyl molecules. For all of the following discussion, crystalline sexiphenyl used to construct the surfaces and step edges is frozen in place using bulk crystal parameters[38] with molecular orientation predicted by MM3π. Long axes of the sexiphenyl molecules form an angle of 14.5° with the surface normal and molecules are planar within the crystal, closely matching experimental predictions and the conditions used in the paper by Hlawacek *et al.*[8] Freezing the substrate in position significantly lowers the computational effort involved as we can then turn off the π system calculations (which do not directly alter intermolecular energy) for the step edge leaving MM3π solely for the admolecule structure. The intermolecular forces between admolecule and step then are described as usual by the standard and computationally efficient Buckingham and Electrostatic parts of the MM3(π). This relies on the assumption that the step edge is a structurally sound and robust entity that does not fragment as the admolecule passes over. To ensure that

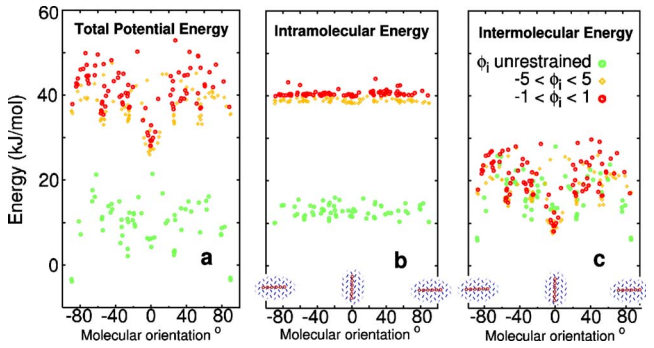

FIG. 5. (Color online) Binding energies as a function of molecular orientation on the (001) surface. The binding energy (or "total potential energy") shown in (a) is the sum of the intermolecular energy, shown in (b), and the intramolecular energy, shown in (c)

freezing molecules in place does not affect the calculation of the barrier to any great extent, a test case involving pentacene, rather than sexiphenyl, was undertaken where substrate molecules were free to move within minimizations. As shown in Appendix C, the difference in barriers for systems in which the substrate molecules are either "frozen" in place or free to move under the influence of the intermolecular forces was under 5 kJ/mol.

1. Binding on (001) surface

To define the energetic baseline for the Schwöebel barrier, we first must know the minimum binding energy on the bulk (001) surface. A search was carried out by generating hundreds of random configurations on the frozen surface and then minimizing the total energy with MM3π applied to the admolecule only. We also conducted simulations in which we constrained ϕ_i to lie within $\pm 1°$ and $\pm 5°$, essentially increasing the rigidity of the sexiphenyl molecule and pushing it closer to the domain of molecules such as pentacene and diindenoperylene (DIP), in order to examine the effect of planarity on the potential energy surface. Figure 5 shows all locally minimized energies as a function of molecular orientation on (001) and demonstrates the multiplicity of available energies, and that this richness resides in variations in the intermolecular energy, not surprisingly. For constrained structures, ϕ_i takes, in the vast majority of cases, the maximum constraint allowed (i.e., $|\phi_i| = 1°$ and $5°$) while for the unrestrained cases $|\phi_i|$ lies between 20° and 40°. The minimum ΔE_{bind} on the surface for the unrestrained molecules is 113 kJ/mol with $|\phi_i| = 36.5 \pm 0.5$ along the molecule and an alternating twist, and its long molecular axis aligned in the [100] direction. For constrained cases, the minimum structure for $|\phi_i| = 1°$ has a value for $\Delta E_{bind} = 111$ kJ/mol and, for $|\phi_i| = 5°$, $\Delta E_{bind} = 112$ kJ/mol. While differences in binding energies are small (1–2 kJ/mol), the effect of constraints on the preferred orientation is dramatic. The minimum energy structure switches from an orthogonal (to [010]) position for the unconstrained case, to a *parallel* position for molecules constrained to be planar within 1° and 5°. This critical result is obtained because the unrestrained molecule was able to access configurations, prohibited to planar molecules, in which the intermolecular interactions are greater. The implications of this result within a NEB search are substantial and important due to the sensitivity of an NEB search on initial and final positions. The sheer number of similar energy local minima on the (001) surface demonstrates the difficulties that will be faced when searching for a saddle point when a step edge is introduced.

2. Trajectory search

For the trajectory search, we constructed a $6 \times 12 \times 1$ supercell step edge containing 144 sexiphenyl molecules with periodic boundary conditions imposed in the [010] direction. (There are actually two subtly different step edges which we use due to the presence of two molecules in the unit cell and depending on which molecule is defined at 0 0 0; for a clarification see Appendix B). A single sexiphenyl molecule was placed on the (001) surface with random orientation and random position (at least 30 Å from the step edge). The total energy of this setup was minimized with the TINKER "Newton" procedure to a tolerance of 1×10^{-2} kcal/mol/Å. Choosing these randomized starting positions assumes that all locally minimized geometries, as shown in Fig. 5, are energetically accessible from the global minimum without compromising the Schwöebel barrier. In other words, the energy required to pass from the global minimum to any starting position is less than the Schwöebel barrier—a condition which we are confident that we have satisfied. From the starting position, the molecule was then repeatedly translated 0.1 Å directly toward the step edge followed by energy minimization—the minimized configuration from the previous step was used as the starting configuration for the next except with the descending molecule translated by 0.1 Å. During minimization, the molecule was not allowed to move away from the step edge but, any other translational, rotational, or conformational move was allowed. We implemented the Newton minimization scheme (tolerance: 1×10^{-3} kcal/mol/Å) at each step to find the local minimum rather than a more globally effective minimization routine to ensure that we were not bypassing any significant local maxima along each trajectory. Each run produces a possible trajectory of the diffusing molecule over the surface; the trajectory with the lowest additional energy is chosen as the predicted Schwöebel barrier. The many internal degrees of freedom accessible to sexiphenyl render it necessary to carry out a larger number of runs to ensure that we are probing as much configurational phase space as possible.

3. Trajectories constraining ϕ_i

We again examined the effect of planarity by imposing constraints on ϕ_i (unrestrained, and those constrained to ± 1 and ± 5) and, for each constraint case, we examined over 150 trajectories. In Fig. 6, we show the three minimum energy trajectories for the sexiphenyl molecule descending over the step edge, giving overall barriers of 35, 40, and 43 kJ/mol, respectively.[39] It is apparent that constraining ϕ_i affects the trajectory in several ways but does not affect the barrier significantly.

Constraining $|\phi_i| < 1°$, produces a trajectory where the molecule log rolls over the step edge in a parallel orientation.

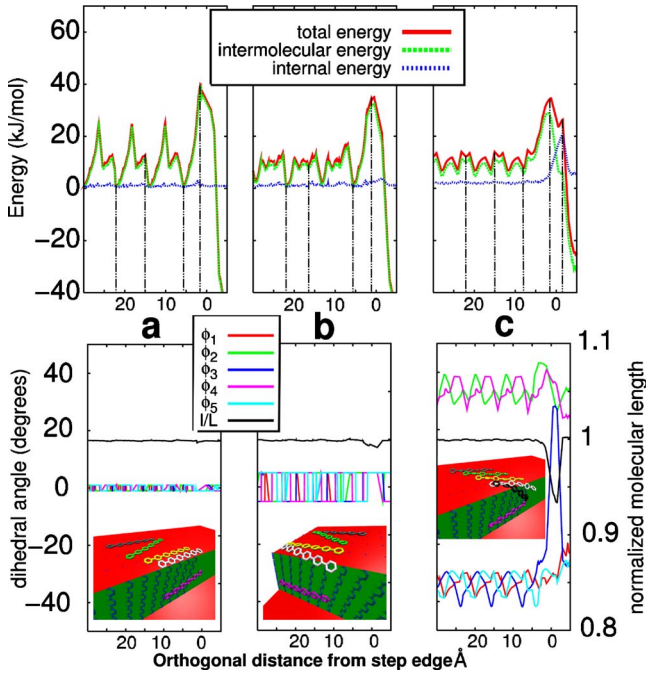

FIG. 6. (Color online) Trajectories resulting in the lowest Schwöebel barrier for three cases restraining ϕ_i: (a) angular rotation constrained to less than 1° ($|\phi_i|<1°$), (b) angular rotation constrained to less than 5° ($|\phi_i|<5°$), and (c) unrestrained molecular rotation. The total energy shown in the plots is the sum of the intermolecular energy and intramolecular energies. The distance axis refers to the orthogonal distance from the center of the middle phenyl ring to the step edge.

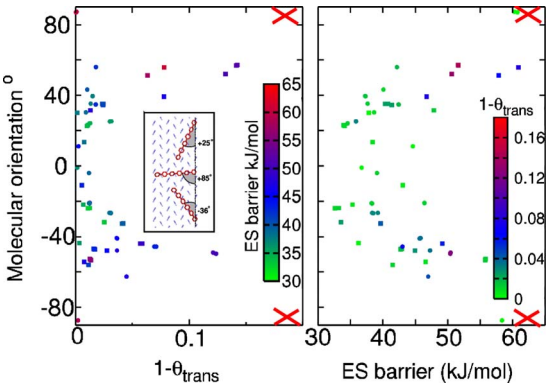

FIG. 7. (Color online) Phase space explored during the Schwöebel barrier search. Data relate to the transition state (i.e., the maximum energy within each trajectory). The left panel shows the angle of approach as a function of bend in the molecule. The right panel shows this as a function of the Ehrlich-Schwöebel barrier. The data are color coded as shown in the bars on the right-hand side of each panel, with green points denoting low values and red ones denoting high ones. Large red X symbols are the results estimated from Hlawacek *et al.*

The molecule remains planar and unbent throughout; therefore, the energetic contributions to the barrier come entirely from the intermolecular energy. We have, in effect, found a Schwöebel barrier for a rigid molecule that is roughly half the 85 kJ/mol value predicted by Hlawacek *et al.* and in which the molecule loses less than 40% of its binding energy to the (001) surface (as opposed to the 70% loss proposed by Hlawacek *et al.*).

By relaxing constraints on $|\phi_i|$ to $<5°$, we see the same log roll approach to the step edge, but, at the transition point, a small degree of bending is now observed. As the molecule twists in a helical conformation, the overall barrier is reduced by 5 kJ/mol. Again, very little contribution to the barrier comes from the internal energy of the molecule.

Only when we lift constraints on ϕ_i completely, do we see more bending of the molecule within the trajectory, yet still only resulting in a normalized molecular length $\theta=0.93$ (i.e., a 7% bend in the molecule). The internal energy of the molecule, corresponding to the reduction in θ, rises (24 kJ/mol) *as* the transition state is reached. At this point, the increased energy of the system resulting from loss of intermolecular interactions means that it becomes more favorable for the molecule to bend and regain intermolecular interactions with the step edge. We also see a change in the configuration of the twisted molecule, with a flip in signs of ϕ_3 as the molecule bends.

From these three cases, ranging from tight constraint to complete unconstraint, the preferred trajectories always involves the molecule log rolling off the step edge. Bending and twisting of the molecule only slightly reduces the barrier by facilitating a complicated "Fosbury Flop"-like mechanism in a near-parallel approach to the step edge. It must be noted that there are many different trajectories for all three cases, although, by constraining ϕ_i, we are enormously reducing the phase space and thus most successful trajectories pass through the same transition points shown in Figs. 6(a) and 6(b); the vast majority of molecules were able to reorient themselves into a near-parallel orientation on the terrace before descending. For the unrestrained case, we observed numerous trajectories of varying energies passing through numerous different transition points.

4. Phase space of unrestrained trajectories

In Fig. 7, we show collated results of over 300 simulations mapping out values of the Schwöebel barrier that can be explored by the molecule as it traverses the step. We plot the orientation of the molecule relative to the step edge at the transition point and the molecule's normalized molecular length. Significantly, all of the barriers predicted by our method are lower than the previously reported prediction in the literature.[8] Figure 7 shows that the lowest-energy trajectories are clustered around two nodes at $\pm 20°$ and $\theta=0.95$ indicating a strong tendency for the molecules to orient themselves more parallel to the step edge as they descend. The same qualitative behavior observed in Fig. 6(c) is seen for all trajectories except that, in general, if molecules approach the step edge more orthogonally, they are unable to bend in this configuration until the driving force (the loss in intermolecular interactions) becomes sufficiently large. The only molecules that underwent significant ($\theta<0.9$) bending at the transition point approached the edge with orientation of around $\pm 50°$ and correspond to relatively high Schwöebel barriers. The lowest value of θ that occurs at the transition point is 0.85 however, as we saw from Fig. 6, the molecule

continues to bend directly after the transition point resulting in a slightly lower θ_{min} for each trajectory. The lowest θ_{min} for all trajectories was 0.825; see Appendix B. We do not see any trajectories in which the molecule continuously drapes itself over the step edge.

We include the value due to Hlawacek *et al.* (60 kJ/mol) on Fig. 7 with the molecule in an orthogonal orientation and an extrapolated value of $0.8 < \theta < 0.825$. It is clear that their result represents a high-energy point within the data set in the much more complex "phase space" that is available to sexiphenyl. It is unclear why parallel orientations were unexplored by their search, particularly in light of our results shown in Figs. 6(a) and 6(b) for rotationally constrained molecules. It could be related to the intermolecular potential energy model they chose but we believe that the most likely reason is that the constraint implicit in the NEB search they employed only examines trajectories directly between the global minima on each surface. Linear interpolation between the initial and final positions, particularly when they are close together, is not guaranteed to explore all of the phase space available to the molecule.

III. EHRLICH-SCHWÖEBEL BARRIERS OF SEVEN COMMON ORGANIC SEMICONDUCTING MOLECULES

We now introduce a further six molecules into this study within which there are two distinct subsets: those in which all rings are fused by sharing atoms (anthracene, tetracene, pentacene, DIP, and C_{60}) and those in which some rings are joined by external bonds (rubrene and sexiphenyl), allowing more conformational flexibility, and hence a more complex conformational phase space. The fused-ring molecules can be considered as almost rigid bodies exhibiting a progression of geometric shape from linear molecules of varying aspect ratio to the spherical C_{60} molecule. All molecules have been experimentally deposited as thin films on a variety of substrates, with varying success from a mobility point of view. Rubrene and sexiphenyl contain four and five bonds, respectively, about which a twist can occur. The extra degrees of freedom these latter molecules possess may be responsible for the fact that it is harder to deposit these molecules in ordered crystalline films than the fused-ring molecules.[40]

A. Molecular step edges

For each molecule, we constructed a step edge using bulk crystal structures.[41–47] While we acknowledge the existence of several thin-film "polymorphs" or "phases" in small organic molecules of this kind (particularly for pentacene[35,36,48,49]) we ignore them in this study. In pentacene, the existence of polymorphs is due to shifts in the alignment of adjacent herringbone layers rather than any significant difference in intralayer packing.[49] Since MM3π accurately predicts an intralayer herringbone arrangement common across the polymorphs and the descending molecule is oblivious to the relative stacking of the layers below due to the large dimensions of the step relative to the range of the energetic potential it is sensible to ignore it. Sexiphenyl on the other hand exhibits a gradual progression from the submonolayer structure to the bulk phase[8] rather than two distinct structures therefore to maintain consistency we concentrate on bulk structures.

All molecules, with the exception of C_{60}, pack in a herringbone structure; their unit-cell parameters are given in Table III. C_{60} packs on a hexagonal lattice. The molecules were minimized within the unit cell using MM3π. The unit cells were then used to construct supercells representing the step edges which can be visualized in Fig. 8. The steps consisted of one layer of molecules (except for C_{60}; method described below) with periodic boundary conditions imposed in the direction parallel to the step edge. The choice of step edge was influenced by the preferred growth orientation of the herringbone structures.

Pentacene, tetracene, anthracene, DIP, and sexiphenyl are almost indistinguishable in the view down the molecular axes and, as a consequence, the (001) surfaces will be energetically similar for any absorbed molecule. The most useful form of these substances in thin-film applications occurs on dielectric or inert substrates with the (001) plane parallel to the substrate and orthogonal to the direction of growth. This growth sometimes occurs naturally on dielectric or inert substrates as with pentacene and DIP (Ref. 50) but, for others, it can be promoted by the presence of buffer layers. For the linear molecules, all unit cells, except DIP, are defined with [100] (*a* axis) as the long axis in the *xy* plane. In DIP, the [010] direction (*b* axis) is the longer. From previous work on surface energies of pentacene, oligioacenes, and oligiophenylenes[34,51,52] it is known that the (100) surface is the more stable of the two. The other surfaces predicted and observed in the equilibrium thin-film growth of pentacene and sexiphenyl are (110) and $(1\bar{1}0)$. For consistency, we choose the same direction in relation to the herringbone structure for all molecules. The step edge is parallel to the furrows of the herringbone structure when viewed down the molecular axis.

The step edge chosen for rubrene follows the logic of the previous choice consistent with the herringbone structure. Although rubrene is notoriously hard to grow in a crystalline thin film, it has recently been shown to grow where the *a* axis of the rubrene unit cell is perpendicular to the substrate surface on a buffer layer of pentacene[53,54] with good crystallinity. Here the (010) surface is equivalent to the top surface in the other crystals and the (001) surface is parallel to the furrows created by the herringbone structure.

For C_{60}, the choice was more arbitrary yet simpler due to the symmetry of the molecule. The step edge is constructed from the bulk fcc structure of C_{60} and we start molecules on the (111) surface and move them toward a $\{\bar{1}11\}$ microfacet.

Complications for sexiphenyl and rubrene also arise from the question of molecular planarity within the film crystal structure. Both molecules form herringbone-type molecular crystals, yet they exhibit different conformations in the crystalline state related to that of the isolated molecule, due to the increased intermolecular interactions in the crystal structure.[24,26] For both molecules, there is still no consensus regarding the degree of planarity within these films. Paraskar *et al.*[26] claim that the molecular tetracene backbone of rubrene is only planar in bulk crystals and not necessarily in

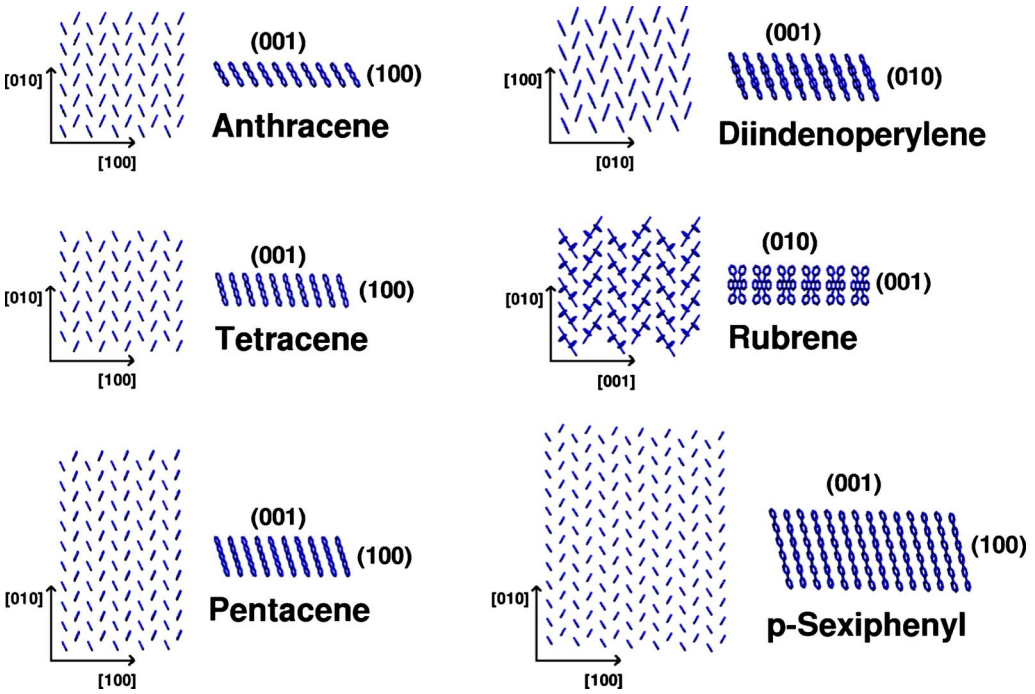

FIG. 8. (Color online) Step edges studied. In each case the step edge is viewed down the molecular axes (from above), highlighting the herringbonelike structure of the crystals and along the direction of the step edge.

thin films (although the deviation is only slight). The twist over the entire tetracene backbone for an isolated molecule is predicted to be roughly 35° by the MM3π potential, comparing well to the value of 42° found using B3LYP calculations by Paraskar *et al.* The previous section discussed the degree of planarity of sexiphenyl where the isolated molecule is twisted about its long axis and that the crystal structures are, on average, planar. The research community interested in small organic molecule seems slightly unsure how to deal with this. For this work, both the tetracene backbone of rubrene and the entire sexiphenyl molecule are considered to be planar when in the crystalline step-edge environment. This is not an assumption but a computational observation when a cluster of proximal molecules are considered; planarity is predicted by MM3π when the geometries are minimized within the bulk crystal unit cells.

B. Binding energies

Calculation of maximum binding energies between top surfaces of steps and descending molecules was achieved as before by generating hundreds of random starting configurations and performing a full energy minimization with the molecules in the crystal frozen in place. Values of ΔE_{bind} are shown in Table II. All molecules preferred to lie as flat on the surfaces as possible, maximizing the interaction with the surface—this is obviously easier for planar molecules. With rubrene and sexiphenyl the strength of the interaction is not strong enough to enforce a planar configuration of the backbone of the admolecule. The density of local minima is also higher for sexiphenyl and rubrene where the internal degrees of freedom are higher, suggesting that subsequent trajectory searches will be more difficult.

C. Self-Schwöebel barriers

The procedure followed for each search was outlined in the previous section: a molecule was placed on the top surface and pushed continuously (in a sequence of 0.1 Å steps) toward the step edge with total energy minimized at each point. MM3π was employed for the descending molecule

TABLE II. Properties of molecules studied calculated from MM3π-minimized representations.

Molecule	ΔE_{bind} (kJ/mol)	ΔE_{CCE} (kJ/mol)	Length (Å)	Width (Å)	Ratio	Molecular weight (g/mol)
Anthracene	39	83	9.25	5.0	1.85	178
Tetracene	52	107	11.72	5.0	2.34	228
Pentacene	65	131	14.14	5.0	2.83	278
DIP	71	149	15.86	6.64	2.39	400
C_{60}	83	155	7.08	7.08	1.00	720
Rubrene	74	154	13.60	11.75	1.16	533
Sexiphenyl	113	174	25.71	4.26	6.03	459

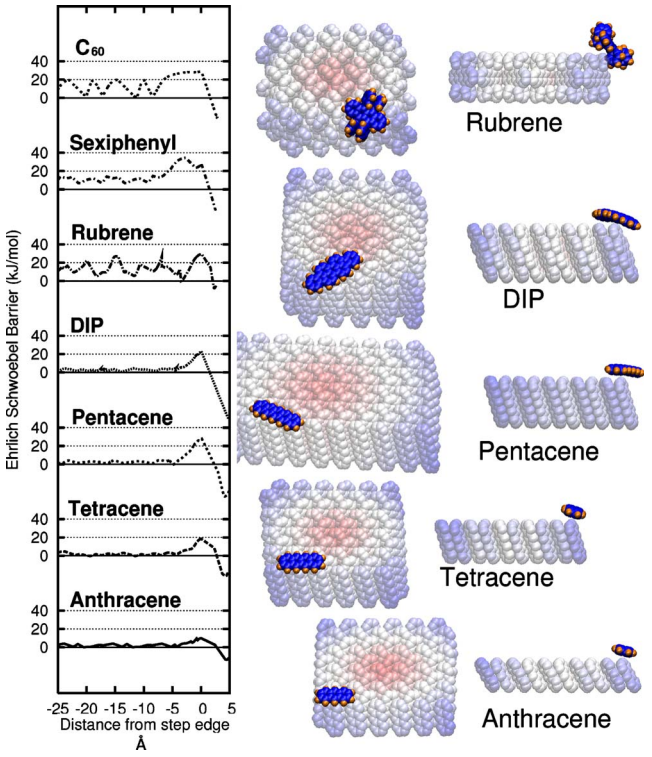

FIG. 9. (Color online) Left: minimum-energy trajectories for the self-Schwöebel barriers of all the molecules studied. Right: corresponding transition point snapshots for the self-Schwöebel barriers of anthracene, tetracene, pentacene, DIP, and rubrene (sexiphenyl is omitted as it was described extensively in the previous section and the conformation of C_{60} is comparatively uninteresting.)

only and all molecules contained within the step edge were frozen in place.

Minimum energy trajectories corresponding to the "self"-Schwöebel barriers for all seven molecules are shown in Fig. 9. The difference between the bottom four trajectories of the planar fused-ring molecules and the top three trajectories is quite striking. The bottom four trajectories (for the linear acenes and DIP) share a similar small ($\approx$5 kJ/mol) 2D diffusion barrier on approach to the step edge, followed by a more pronounced rise in energy at the step edge due to the Schwöebel barrier. In contrast, trajectories for rubrene, sexiphenyl, and C_{60} exhibit larger 2D diffusion barriers on the terrace which are on the same order as rises at the step edge. This is due, in the case of rubrene and sexiphenyl, to the flexibility of the molecules on the surface—the molecules have conformational states available to them which are prohibited to the fused-ring molecules. By allowing small twists and bending of single bonds, rubrene, and sexiphenyl can adapt more easily to subtle variations in the surface and therefore explore lower-energy configurations. The acenes and DIP experience more of a rigid-body interaction with the surface and, therefore, the surface appears energetically smoother. For the six herringbone-type crystals, the top surface on which the molecules are adsorbed is relatively flat in comparison to the molecular length of adsorbed molecules and the large molecular lengths go some way to screening out any variations or corrugations in the surface. The C_{60} barrier is more reminiscent of an atomic system, but on a larger scale; as with atomic systems, the molecular length and the surface corrugations are equivalent, thus, the adsorbed C_{60} molecule is more sensitive to the topological features of the C_{60} surface resulting in higher 2D barriers.

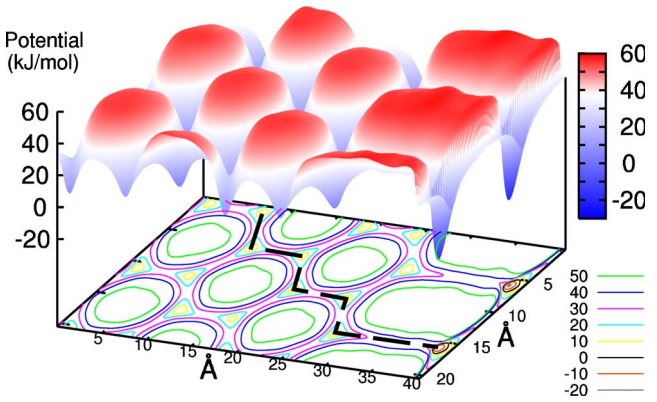

FIG. 10. (Color online) Potential energy surface of the C_{60} Schwöebel barrier. The thick black dashed line traces the trajectory shown in Fig. 9.

1. C_{60} potential-energy surface

Due to the *relative* simplicity of the C_{60} molecule we were also able to map out the entire minimum potential energy surface for a molecule approaching the step edge (Fig. 10). We used a technique recently employed by Cantrell *et al.*[9] where a C_{60} molecule is used to probe the C_{60} surface. A fine mesh of points (with a grid size of 0.1 Å) was generated and the energy minimized with respect to the z coordinate at each point. The internal coordinates of the probe molecule (and rotational degrees of freedom) were frozen and the molecule lowered toward the surface until the potential energy minimum is found. Cantrell *et al.* showed that the rotational degrees of freedom only have a small effect on the potential energy of the system however nonredundant rotational degrees of freedom in all other molecules studied here prevented their effective use as a probe for their respective surfaces. A comparison of Figs. 9 and 10 indicates that the minimum trajectory in the former corresponds to the minimum-energy path through the Potential Energy Surface. C_{60} is also the only case where there exists a clear diffusion barrier that can be separated from the Schwöebel barrier. (Traditional values of each would have ΔE_{diff}=20 kJ/mol and ΔE_{ES}=10 kJ/mol but, for ease of comparison to the other molecular species, we report a combination of the two.) The diffusion barrier compares well to a study by Liu *et al.*[55] where Arrhenius-type behavior is assumed to calculate various C_{60} diffusion barriers from coarse-grained molecular-dynamics (MD) simulations. They inferred a value of ΔE_{diff}=17 kJ/mol for simple 2D diffusion; however, there was no direct comparison available for the Schwöebel barrier.

2. Transition points

Trajectories of the five molecules with aspect ratio above 1.5 share similar modes of descent with transition points oc-

curring with the long molecular axes close to parallel to the step edge (Fig. 9). Only sexiphenyl has the ability to bend significantly and all other molecules we studied may be considered more or less rigid. If these molecules were to approach the step edge orthogonally, the energy penalty would be greater, as more of the molecule would be estranged from the molecular crystal. As reported in the previous section, sexiphenyl is able to bend slightly but the cost of bending around the step edge orthogonally is still prohibitive and therefore a more parallel conformation is observed.

It can be anticipated that rubrene will provide the least reliable estimate of the Schwöebel barrier due mainly to the inherent complexity arising from its conformational freedom. Throughout this work, we observed that the rubrene molecule often experienced a 2D diffusion barrier to traverse the surface that can be of equal or greater magnitude to the Schwöebel barrier to descend the step edge. This presents a conceptual problem: the major assumption that all local minima on the top surface are energetically available at a cost lower than the Schwöebel barrier may not hold for highly and dynamically nonplanar molecules such as rubrene. Due to its lack of planarity, the rubrene molecule is not as geometrically bound to the surface (in the sense that there is not a clear energetic advantage to lie on the surface in one particular orientation since the rest of the molecule can adopt so many other nonplanar conformational variations) and thus, overall, rubrene finds steps no less difficult to navigate over than relatively flat surfaces.

3. Correlating Schwöebel barriers to molecular characteristics

In an attempt to understand how the self-Schwöebel barrier is related to physical characteristics of the molecule and, more practically speaking, providing a means to estimate the self-Schwöebel barrier *without* performing these lengthy simulations, we plotted the value of the self-Schwöebel barrier that we calculated as a function of several different geometric and physical characteristics that we imagined might play a role; the results are shown in Fig. 11. The characteristics we chose were molecular length, molecular width, aspect ratio (length to width), molecular weight, crystal cohesive energy, binding energy, and the angle the step forms with the top surface (see Tables II and III).

Examination of Fig. 11 shows there is no simple linear relationship between the Schwöebel barrier and any single metric for the set of molecules studied, though the crystal cohesive energy and binding energy come the closest to providing a linear (or at least a simple) relationship. Several other observations can be made about Fig. 11: (a) the acene homologous series (anthracene, tetracene, and pentacene) shows a large degree of correlation for many of the metrics we selected (b) depending on how you interpret the correlation for a given metric, in general, rubrene and C_{60} tend to be outliers.

The two most promising correlations, the crystal cohesive energy (CCE) and binding energy, both indicate something about the ability of the molecule to form favorable interactions (within the crystal and on the top surface, respectively). A linear correlation with these variables suggests that the Schwöebel barrier is a function of the original interaction

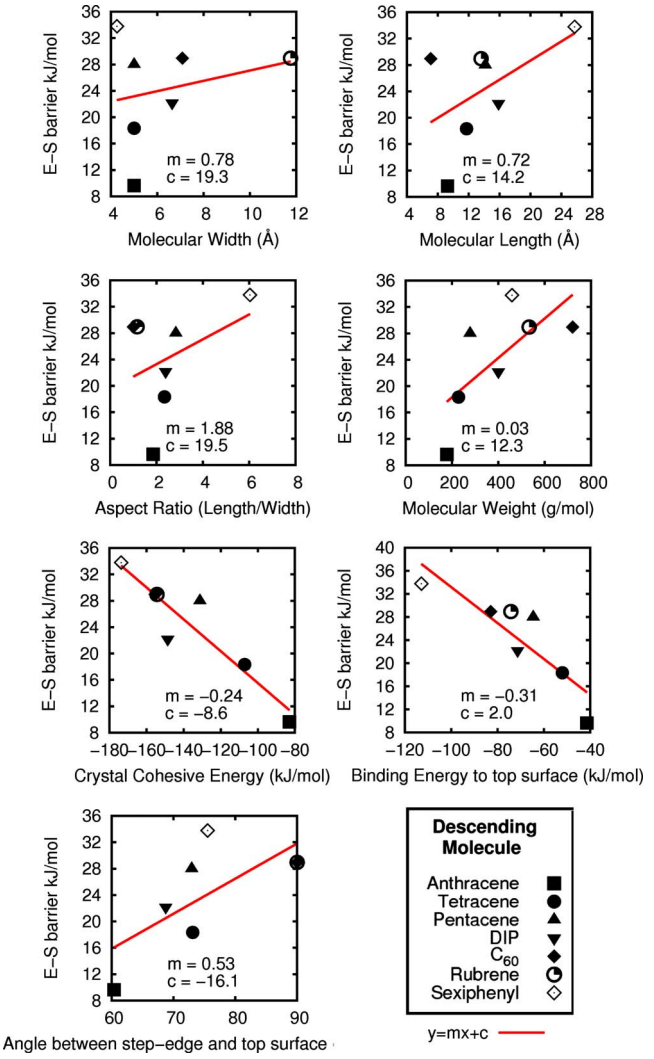

FIG. 11. (Color online) Correlations of the self-Schwöebel barrier against seven molecular variables.

strength and that the molecule will always have to lose a certain proportion of that energy (30% in the case of the binding energy) as it navigates the step edge. DIP and pentacene are the only molecules that produce qualitatively inaccurate predictions based upon these metrics, i.e., DIP has a higher binding energy/CCE than pentacene but produces a lower barrier. The deviations from best fit lines are less than 5 kJ/mol in the case of the binding energy correlation.

D. Heterostep-edge barriers

While step-edge barriers that a molecule experiences as it traverses a surface composed of its own type are important, there are many important real-world situations where the morphology of an interfacial layer between dissimilar materials, a heterointerface, plays an important and, perhaps a critical, role in determining the properties of the device. Heterostep-edge barriers are of particular importance, for example, when considering the growth of organic heterojunctions for use in photovoltaic devices. Recent research has focused on using C_{60} as the acceptor layer, with a variety of other molecules as the donor.[56–58]

TABLE III. Unit cells dimensions of molecular crystals.

Molecule	**a** (Å)	**b** (Å)	**c** (Å)	α	β	γ	**m**	Angle[a]
Anthracene	8.56	6.04	11.16	90.0	124.7	90.0	2	60
Tetracene	7.90	6.03	13.53	100.3	113.2	86.3	2	73
Pentacene	7.90	6.06	16.01	101.9	112.6	85.8	2	73
DIP	7.17	8.55	16.8	90.0	92.42	90.0	2	69
C_{60}	14.17	14.17	14.17	90.0	90.0	90.0	4	90
Rubrene	26.86	7.19	14.43	90.0	90.0	90.0	4	90
Sexiphenyl	8.09	5.57	26.24	90.0	98.17	90.0	2	76

[a]The angle formed between the planes of the top surface and the step edge.

In an attempt to broaden the concept of step-edge, Schwöebel, barriers we calculate the hetero-Schwöebel barriers of all seven molecules studied in Fig. 1 on four surfaces that we have already studied in some detail—namely, pentacene, tetracene, DIP, and rubrene. There are no calculations in the literature of hetero-Schwöebel barriers. Pentacene and tetracene were chosen because of the similarities in their unit cells and crystal structure—we expect to find almost identical results between the two but select them to confirm that we can predict when surfaces will behave similarly. The behavior of DIP and rubrene differ significantly from the acenes and provide enough variety to justify any postulated correlations of hetero-Schwöebel barriers.

We also studied a different pentacene step edge from the one studied in the preceding section. This second pentacene step edge, which we will call pentacene-α, was included to test the effect of the precise type of step edge that a descending molecule may encounter, an effect that was not considered in the preceding section for pentacene. The only difference between the two pentacene step edges is exactly which molecule in the unit cell forms the step surface; see Fig. 12. This difference in step edges was considered for sexiphenyl as described in Appendix B and depends on which of the {100} planes is chosen to cut the step edge.

Correlations of Schwöebel barriers with physical metrics

The introduction of hetero-Schwöebel barriers means that any successful metric used to correlate the barriers across different molecular systems is likely to include information about both the molecule descending the step edge and the nature of the step edge itself. Referring to our experiences with self-Schwöebel barriers in the preceding section and the correlations across molecule types, the only metric which satisfies this concept of including the crossinteraction of the diffusing (ultimately, descending) molecule and the underlying surface is the binding energy of the descending molecule to the top surface. (This was one of the most promising correlations for the self-Schwöebel barrier determined in the preceding section.) While another option could be a combination of two or more of the other metrics we considered, our results with the binding energy were sufficiently encouraging to preclude any such study at this time.

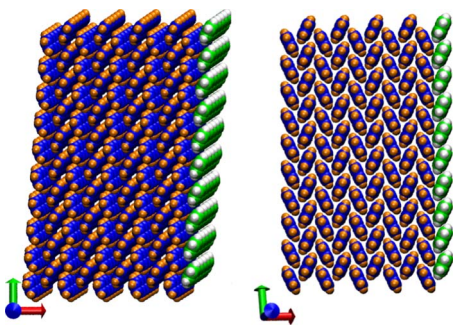

FIG. 12. (Color online) Depiction of the two different types of pentacene step edges. The exclusion of the green and white molecules creates a different orientationally disposed step edge (pentacene-α) to that if the green and white molecules are included (pentacene-β). The step edges are shown as views from directly above (left panel) and down the molecular axes (right panel).

In Fig. 13, we show correlations of both the self- and hetero-Schwöebel barriers versus the binding energy for all seven diffusing/descending molecules over each of the four different surfaces (pentacene, anthracene, rubrene, and DIP). The roughly linear correlation of binding energy with Schwöebel barrier held up well across all surfaces. There is also a consistently linear relationship within the acene homologous series across all surfaces. Encouragingly, the results for all seven targeted molecules are almost identical for the pentacene and tetracene surfaces (except when rubrene is the descending molecule). The results also show that, as a general rule, the size of the step-edge barrier for sexiphenyl is consistently and significantly lower than its binding energy to the surface suggests. We attribute this departure to its ability to bend and adapt its conformation as it navigates the step edge. This is responsible for skewing the linear fit away from the other molecules for the tetracene, pentacene-α and pentacene-β surfaces, in particular. The difference between the steepness of the correlations for the two pentacene surfaces (α and β) highlights the complexity of the system we are dealing with and the sensitivity of the barriers to slight changes in the step-edge topology.

There are two points of concern among this data: first, the roughly 13 kJ/mol discrepancy between the Schwöebel barriers for rubrene on tetracene and rubrene on pentacene and, second, the higher than expected barrier for DIP on rubrene. That rubrene should be involved in both of these unexpected results should not be a surprise considering it is conformationally the most complex molecule we studied. The low value of the Schwöebel barrier of rubrene on tetracene is a case where the Schwöebel barrier that we calculated for this

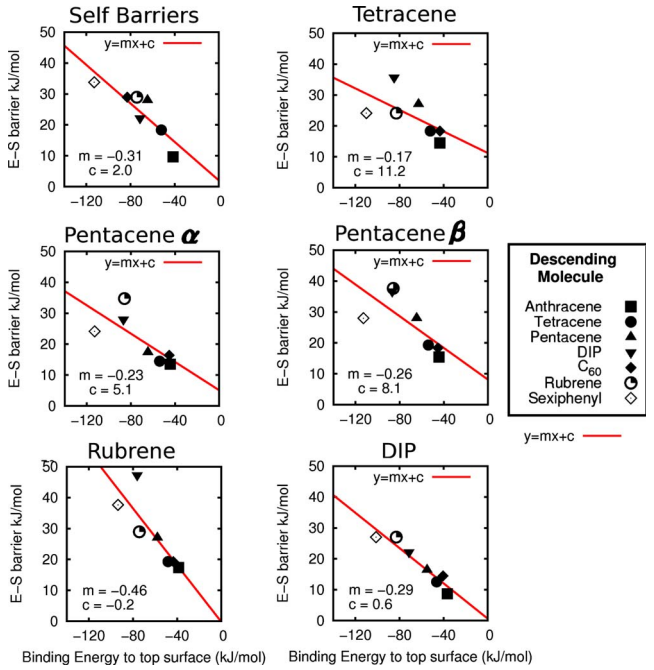

FIG. 13. (Color online) Correlation of the Ehrlich-Schwöebel barrier with the binding energy on the top surface for the self-Schwöebel barriers and hetero-Schwöebel barriers. The bold title on each subfigure refers to the type of surface and step edge over which the adsorbed molecule is descending. The barrier for each of the seven descending molecule types is shown on every surface using symbols provided in the accompanying key on the right-hand side.

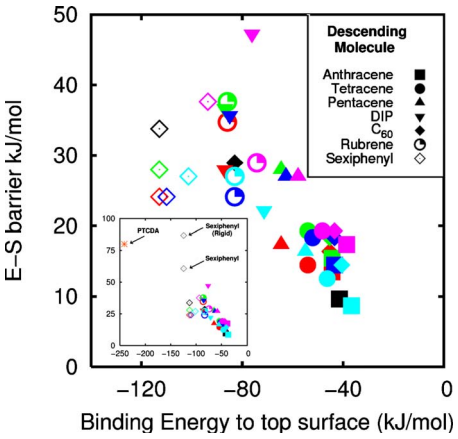

FIG. 14. (Color online) Relationship between binding energy and Schwöebel barrier for the set of systems studied in this work. The color of the points refers to the material constituting the step edge; the point style denotes the descending molecule (see key). Black—Self-barrier; dark Blue—tetracene, red—pentacene-α, green—pentacene-β, magenta—rubrene, and light blue—DIP. Inset: inclusion of previous results in this field. Gray shows the results for sexiphenyl from Hlawacek *et al.* and orange denotes the results for PTCDA from Fendrich *et al.*

trajectory is lower than some of the 2D diffusion barriers we observed for other trajectories of rubrene on tetracene and so the concept of a Schwöebel barrier is not really applicable.

In Fig. 14 all our results are consolidated onto one graph of Schwöebel barrier versus binding energy in pursuit of a universal relationship. The inset includes results from the only other previously reported values of Schwöebel barriers for organic molecules (for PTCDA and sexiphenyl); the PTCDA result would lie on a linear relationship through our data but the result for sexiphenyl does not. Our concerns over the sexiphenyl results have already been thoroughly discussed in the preceding section. Although we can correlate the binding energy with the Schwöebel barrier reasonably well over the entire range of systems studied within an uncertainty of about 10 kJ/mol or less, there are clearly other variables contributing toward the Schwöebel barrier. For example, rubrene step edges consistently give higher Schwöebel barriers than DIP step edges. We can postulate reasons for this, although quantification becomes problematic. One of these variables is the angle which the step forms with the top surface. This was investigated by Hlawacek *et al.*[8] for the sexiphenyl system where a gradual standing up of molecules was observed experimentally from the first monolayer upwards until bulklike conditions were observed. It is intuitive that the more severe an angle that the step forms with the surface (i.e., the more upright the step edge), the higher the barrier. However, we have yet to quantify this with all of our results due to the difficulty in defining a "step angle." Because the steps are constructed of molecules which are not geometrically simple (especially in the case of rubrene) the surfaces that they form exhibit local variations (i.e., deviations from the surface plane) over the range of one unit cell thus complicating the measurement. The crystals can be thought of as exhibiting a fractal dimension greater than unity—depending on the scale of measurement the angle varies. For example, as can be seen from Fig. 8, on a macroscale the angle between (010) and (001) for rubrene is clearly 90° whereas on an Å scale this is not the case and there is considerable variation along [010]. However it is clear, again from Fig. 8, that the rubrene step presents a more severe angle than DIP.

IV. MOLECULAR DYNAMICS: PENTACENE

As an extension to the above calculations we also carried out molecular-dynamics simulations probing the pentacene self-Schwöebel barrier at 300 K with the step-edge molecules free to move. The increased demand on computational power needed to describe the time evolution of system necessitated the use of the MM3 potential for the entire system. The use of molecular dynamics to study energetically activated processes in such a complex phase space is always challenging and it is almost impossible to extricate any meaningful quantitative information from a single simulation, however, by propelling a pentacene molecule toward the step edge and allowing the system to evolve under an NVE (microcanonical) ensemble we observed numerous trajectories qualitatively consistent with our previous calculations. The most important finding from the molecular-dynamics simulations was that the step edge was not compromised by the descending molecule and maintained its structural integrity throughout thus justifying the assumption

of a frozen step edge in the previous Schwöebel barrier search. Full details, along with some representative trajectories, can be found in Appendix C.

V. CONCLUSIONS

This is a comprehensive study of the Schwöebel barrier of seven small organic molecules on a number of different underlying surfaces, and an attempt to try to link Schwöebel barrier and the physical characteristics of the molecule. As a result of this study, we make several important qualitative observations, which we believe lead to a better understanding of the processes involved in step-edge descent. Perhaps the two most important of these observations is (1) that the Schwöebel barrier for organic molecules is a more complex, richer, situation than for atomic systems and the barrier is a multiplex rather than a single value and (2) that a roughly linear correlation was found between the binding energy and Schwöebel barrier, enabling researchers to estimate the Schwöebel barrier for either self- or heterointerface situations without the need to perform the time-consuming and rather demanding molecular simulations described in this paper.

In general, the molecules lose about 40% of their binding energy as they descend a step edge but this can be reduced in the case of molecules with flexible backbones, such as sexiphenyl. A log-roll mechanism was confirmed as the preferred step-edge descent in which the long molecular axis remains nearly parallel to the step edge. This mechanism is preferred for high-aspect ratio molecules.

Specifically for the self-Schwöebel barrier of sexiphenyl, we find that the molecules prefer to roll over step edges in a parallel orientation. Allowing rotation around the C—C single bonds vastly increases the phase space of the search and results in a slightly lower-energy trajectory where the molecule experiences a kind of "Fosbury flop" at an angle of about 20° to the step edge (interestingly, at roughly the same angle preferred by human high jumpers). The sexiphenyl molecule remains twisted as it descends the step edge, retaining torsional angles of 35°–45°. Nearly all of the energetic contribution to the barrier comes from a loss of intermolecular interactions as the unbent molecule tries to navigate the step edge. Only a small degree of bending occurs at the step edge and a slight rearrangement of the torsional angles to facilitate the descent and reduce the loss of intermolecular interactions. The lowest-energy barrier we found was 32.5 kJ/mol, which is significantly lower than that reported by Hlawacek *et al.* It was also apparent that previous techniques and assumptions based upon atomic systems do not necessarily hold for systems such as sexiphenyl. The sheer number of local minima on the potential-energy surface of the (001) surface that we have uncovered create particular problems for a nudged elastic band method when trying to navigate between the global minimum on the terrace and the global minimum bonded to the step as the potentially tortuous route through a number of local minima is not guaranteed to be discovered.

Although most of the studies in this paper consider the Schwöebel barrier of molecules descending one particular type of step edge, our limited study of different step edges showed that the steepness (as in the DIP step) and even subtle differences in molecular orientation can have a significant effect on the value of the Schwöebel barrier. It is obvious that the features of the step itself play an important part in determining the magnitude of the barrier. So it is likely that other steps or kink sites should play an important role in the evolution of the film. This would be particularly apparent in the submonolayer regime of film growth as the small islands which form would not have particularly well-defined step edges. It also points to the difficulty of a comparison of experimentally derived estimates of step-edge barriers which have to arise from an ensemble average of different Schwöebel barriers depending on the details of the island density and type, and computationally calculated energy profiles of specific ideal step-edge descents. In addition time lapses between the deposition of the molecular thin film and the collection of the AFM data is liable to produce some reorganization of the molecular film which has been shown to be particularly dependent on the time of removal from a low-pressure environment to ambient conditions.[59] For these reasons we would not necessarily expect a close agreement between our minimum energy trajectory (32.5 kJ/mol) for sexiphenyl and the *experimentally* determined value of ≈ 60 kJ/mol in the Hlawacek paper. Thus, experiments and simulations offer quite different sets of information: Simulation is currently the only way to get a precise determination of a particular Schwoebel barrier but is limited by the variation and occurrence of different types of step edges that occur in a typical sample (if such exists). Indirect experimental values are an average over all types of step edges and hence it is not clear what this value represents in the absence of detailed information on the extant step edges in the sample.

ACKNOWLEDGMENTS

The authors are pleased to acknowledge funding from the National Science Foundation's MRSEC award administered to Cornell through the Cornell Center for Materials Research. E.L.F. was funded through Cornell's undergraduate research program, Engineering Learning Initiatives, with a gift from Intel Corporation.

APPENDIX A: TORSIONAL POTENTIALS

1. Torsional potential of biphenyl

Biphenyl has become something of a *cause célèbre* when considering the ability of electronic-structure calculations to predict the geometry of isolated molecules because this relatively simple molecule does not behave as would be expected and the task of explaining this has been given a considerable amount of effort by researchers. The relatively large amount of published literature proved very helpful when interpreting our results and predicting the accuracy of the larger sexiphenyl system. Because of the internal rigidity of the phenyl rings, the complete minimum energy structure can be summarized by one value—the torsional angle between the two phenyl rings (ϕ_{min}). It has been suggested that this angle is thought to be defined by the competing contri-

butions of steric hindrance within a planar molecule and the tendency of the conjugated π system to prefer planarity. Yet even this is debatable.[60]

Sexiphenyl being in the same homologous series as biphenyl can be thought of a series of five of these torsional potentials. A combination of electronic-structure calculations[27–32,60,61] and experimental measurements[62,63] examining the torsional potential of biphenyl have highlighted the strong dependence of the predicted values ΔE_0, ΔE_{90}, and ϕ_{min} on the choice of theory and basis set used in the calculation. The MP2 level of theory which is normally the chemistry of choice for organic molecules performs unexpectedly poorly. It predicts the incorrect relative magnitude of ΔE_0 and ΔE_{90}, and gives a general overprediction of both values of ΔE by this large basis set, sophisticated theory calculation. The values for ϕ_{min} are generally within an acceptable range. Most recently, Johansson *et al.*[27] have examined the simple biphenyl system in great detail and have reproduced the latest experimental values[62,63] through a very sophisticated treatment and a comprehensive analysis of the theoretical errors and their origins. One of the important conclusions is that some DFT methods (i.e., B3LYP) agree well, although probably fortuitously, with the highest-level extrapolated *ab initio* results and experiment. From a practical point of view, this enables relatively accurate calculations to be carried out at far less computational cost.

2. Torsional potential of sexiphenyl

For the longer sexiphenyl molecule, there seems to be consensus that, while neighboring phenyl rings are twisted along the molecular axis of *isolated* molecules,[24,64–66] these torsional angles are reduced when the molecules are packed together into a crystalline environment.[24,38,65,67–69] This effect has also been observed with other conjugated molecules of similar size:[26] an *ab initio* study of poly(*para*-phenylene),[67] for example, predicts a torsional angle of $\phi_{min} \approx 27°$ and a $\Delta E_0 \approx 6$ kJ/mol. Previous estimates of ϕ_{min} in an isolated sexiphenyl molecule lie between 30°–40° using empirical potentials[64,65] and, very recently, using DFT methods[66] with, among others, the same Perdew-Burke-Ernzerhof functionals used by Hlawacek *et al.*

3. MM3π calculation of torsional potentials

The MM3(2000) potential developed by Allinger was parametrized using the structural data of a large number of small organic molecules (biphenyl being among them) but the difficulties in predicting this structure using a simple potential are evident. Without including the MP2 correction for electron correlation (denoted as MM3π), the MM3 potential fails to capture the twisted nature of the molecule and predicts a planar minimum (as it does for sexiphenyl). A dramatic improvement is observed with the inclusion of the MP2 correction although this significantly increases the computational complexity due to the introduction of self-consistent-field iterations. A computational penalty of MM3π over MM3 is about a factor of 100 in CPU time.

We used MM3π to calculate the torsional potential of biphenyl and the torsional potential of the terminal phenyl ring on an otherwise planar sexiphenyl molecule (Fig. 15 and Table IV) and found that MM3π performs as well as the best *ab initio* calculations in the prediction of ΔE_0 and ΔE_{90} and reasonably well in ϕ_{min}. However, the slight underprediction of ϕ_{min} is not critical due to the shallowness of the torsional potential around the minimum. It is interesting to note that the maximum energy configuration does not occur exactly at the planar state but instead with a torsional angle of 80°. When the torsional potential of the terminal phenyl ring on an otherwise planar sexiphenyl molecule is considered, ΔE_0 (6.0 kJ/mol) was found to be very close to the value calculated for biphenyl (6.3 kJ/mol), suggesting the independence of neighboring twists for the straight molecule, with each twist contributing one-fifth to the total $\Delta E_{p\text{-}t}$=30.0 kJ/mol for sexiphenyl. This has been observed by Lukeš *et al.*[66] using DFT methods where only small variations in ϕ_{min} were seen over a range of *para*-phenylene oligomers.

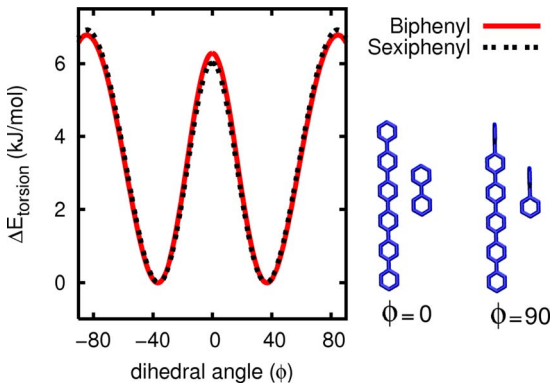

FIG. 15. (Color online) Torsional potential calculated with the MM3π potential for biphenyl and sexiphenyl. Constrained geometry optimizations were performed at ϕ intervals of 1°.

APPENDIX B: SEXIPHENYL-FURTHER ANALYSIS

1. Dissimilar (100) step edges

A further complication in the case of sexiphenyl (and organic molecules, in general) arises due to the number of molecules in the monoclinic unit cell and the subtle difference in their orientation. Each {100} surface exposes only one of the two sexiphenyl molecules in each unit cell, so, depending on which molecule is defined at 0 0 0, the (100) surface is cut differently, producing a slightly different step

TABLE IV. Torsional energy barriers for the biphenyl molecule comparing experimental values to results using a semiempirical potential model, MM3π and *ab initio*-based estimates.

Model	ΔE_0 (kJ/mol)	ΔE_{90} (kJ/mol)	ϕ_{min} (°)
Experiment[a]	6.0 ± 2.1	6.5 ± 2.0	44.4
MM3π	6.3	6.6	35.8
"Best estimates"[b]	8.0	8.3	45.8

[a]Taken from Refs. 62 and 63.
[b]Taken from Ref. 27.

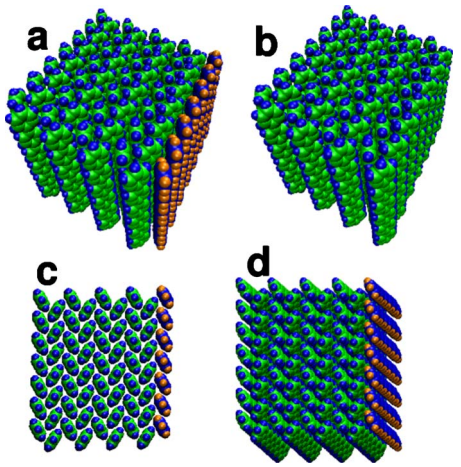

FIG. 16. (Color online) Two possible step edges in sexiphenyl, illustrated by the presence or absence of the final row of different colored molecules. (a) sexiphenyl-α step edge, (b) sexiphenyl-β step edge, (c) the view down the long molecular axis, and (d) the view perpendicular to the a and b axes.

edge (see Fig. 16). We arbitrarily denote the step shown in Fig. 16(a) as sexiphenyl-α and the step shown in Fig. 16(b) as sexiphenyl-β. Hlawacek *et al.* appeared to exclusively use sexiphenyl-β.

2. Sexiphenyl on sexiphenyl: Effect of step edge on trajectory search and phase space

We used both step edges in our search for the Schwöebel barrier and found a small difference between the two although this not as significant as we have found for other organic molecules. The lowest barrier we report (32.5 kJ/mol) was representative of sexiphenyl-α, whereas the lowest barrier for sexiphenyl-β was 35 kJ/mol (see Fig. 17). The sexiphenyl trajectories shown in Fig. 6 were all obtained for sexiphenyl-β steps for consistent comparison with previously published material; however, it can be seen from Fig. 17 that the minimum-energy trajectories for the two different steps edges are very similar. Indeed, the angles of approach are equivalent, though sexiphenyl-α produces a trajectory with slightly less bending of the molecule and the molecule undergoes an extra flip within the torsional angles at the transition point.

Further to Fig. 7, we show the trajectory phase space of the Schwöebel barrier search in terms of the maximum degree of bending of the molecule over the trajectory; the Schwöebel barrier and molecular orientation at the transition point are plotted against $(1-\theta_{min})$ instead of $(1-\theta_{trans})$ in Fig. 18. On both this figure, and Fig. 7, we plot data from both sexiphenyl-α (square points) and -β (circle points) step edges. This difference was not highlighted in the main article so as not to overly confuse the reader.

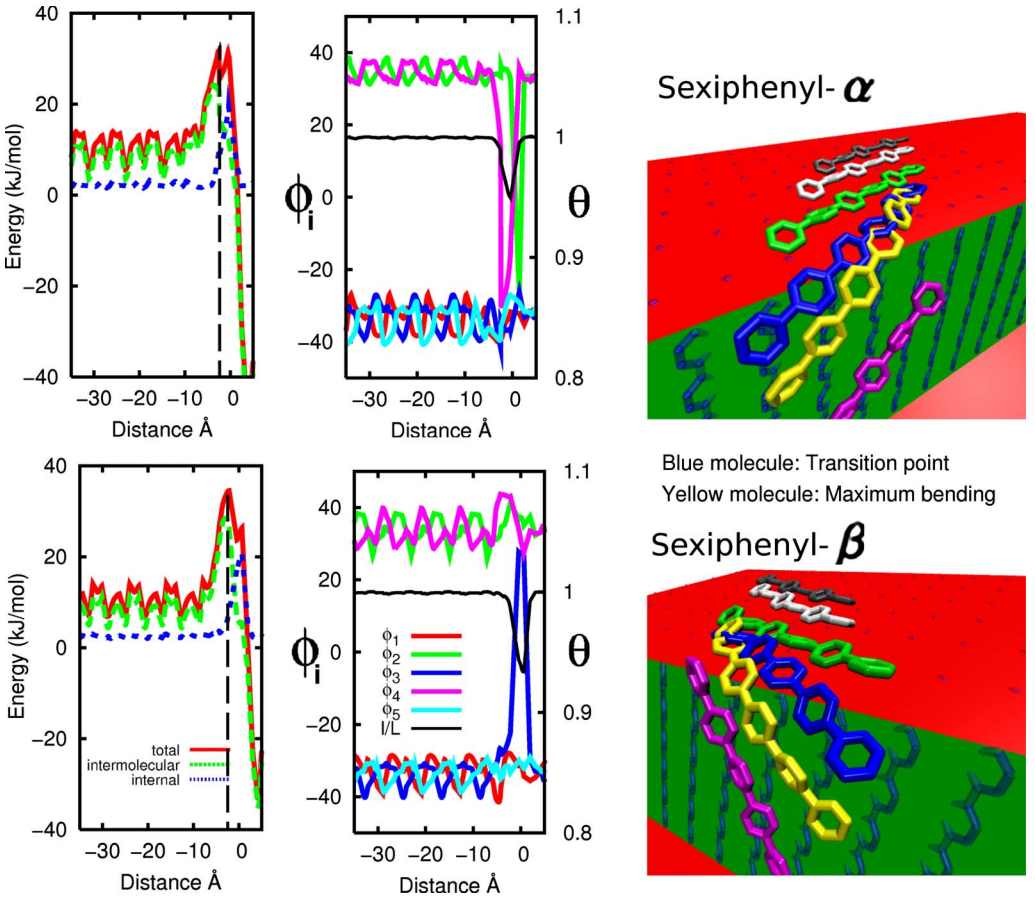

FIG. 17. (Color online) Detailed examination of each of the two minimum trajectories for the two step edges. The distance axis refers to the orthogonal distance from the step edge and the vertical black dashed line shows the transition points corresponding to the blue molecules. The yellow molecules show the maximum bending throughout the trajectories.

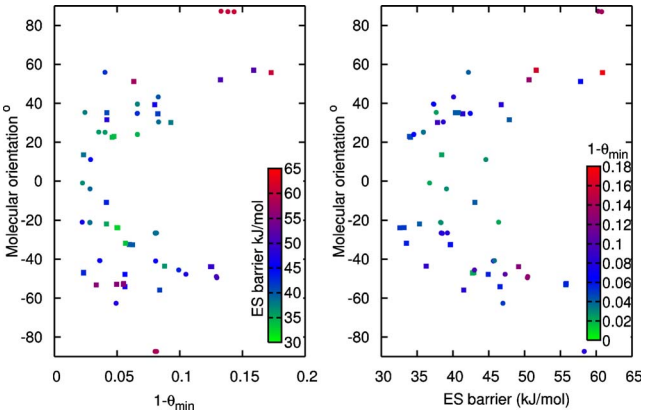

FIG. 18. (Color online) Phase space explored during the Schwöebel barrier search. All θ values are given at the instance of maximum bending of the molecule over the trajectory ($\theta=\theta_{min}$). Square points refer to the sexiphenyl-α step while circle points refer to the sexiphenyl-β step.

3. Orthogonal molecules tethered around the step edge

In order to ascertain, on a fundamental level, whether the MM3π potential model could ever allow a trajectory in which the molecule was continually bent over the step edge we sampled many possible transition states by forcing molecules to bend around the step edge in near-orthogonal configurations (angles $>80°$), at random positions of descent, and evaluating the minimized, locally constrained, geometries. In all, over 4000 states were generated by conducting NVT simulations at elevated temperatures (500 K) followed by energy minimizations. At every position along the transition path, there should be a configuration with energy less than or equal to 60 kJ/mol and, assuming that all neighboring states are energetically accessible, the trajectory becomes possible. It can be seen from Fig. 19 that this condition can be met if the molecule bends around the step edge with $1-\theta=0.18$ but it incurs a high-energy barrier (indeed the maximum observed) of around 60 kJ/mol ($\pm\approx 10$ kJ/mol).

4. Sexiphenyl on DIP

As discussed in the main article, when sexiphenyl is the descending molecule it consistently has a lower Schwöebel barrier than that predicted by the correlation we found with binding energy. The flexibility of the sexiphenyl molecular backbone allows the molecule to navigate the step edge more easily than might be experienced by a more rigid molecule, such as pentacene, say. In the minimum-energy pathway that sexiphenyl seeks to traverse the step edge, the molecule still navigates the step edge with its backbone almost parallel to the step edge. When pentacene, tetracene or rubrene molecules formed the underlying terrace and step, we observed no trajectories where sexiphenyl preferentially oriented itself in an orthogonal approach to the step and none in which the molecule drapes itself continually over the step edge (bending at each C—C bond).

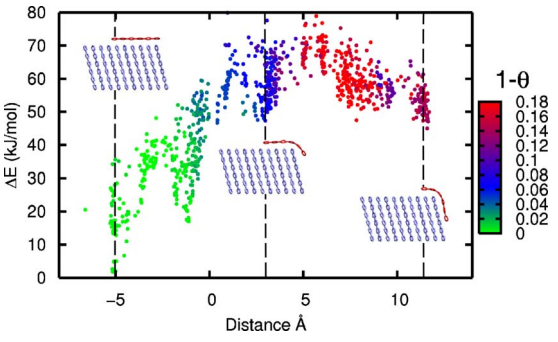

FIG. 19. (Color online) Potential energy (intermolecular +intramolecular) of sexiphenyl molecules forcibly bent over the step edge.

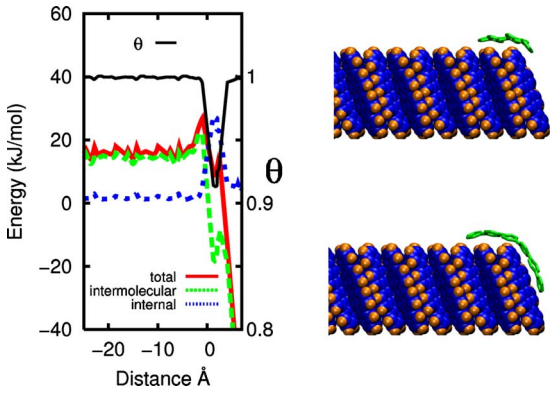

FIG. 20. (Color online) The energetic profile (left) and key snapshots (right) of the minimum-energy trajectory for a sexiphenyl molecule to descend over a DIP step edge. Note the relative invariance of the low-energy path as the molecule traverses the terrace and the relatively small period of energy loss at the transition point.

However, when DIP molecules form the underlying terrace and step, we did observe one instance that produced such a trajectory, leading to a hetero-Schwöebel barrier of 40 kJ/mol. While this descent, featuring a sexiphenyl molecule smoothly draped over the step edge, was not the lowest-energy trajectory (the lowest being 27 kJ/mol), the value of 40 kJ/mol is within an accessible energetic range, and hence in dynamic situations molecules would be anticipated to occasionally adopt this "draped" descent. In Figs. 20 and 21 we examine the energetics of both trajectories. In Fig. 22, we show snapshots of the molecule as it drapes over the step edge. This is an important result in the context of the Hlawacek *et al.* paper as it shows that our search method *is* able to pick up such a trajectory if it is of low-enough energy to occur. The reason that it was seen for DIP and not on other surfaces is because of the shape of the DIP molecule and how it forms step edges. The relatively large molecular width of DIP means that more carbon atoms are exposed at the step-edge face and so the binding energy of the descending molecule is stronger (than it would be on the other surfaces we considered, for instance). When an orthogonally approaching molecule begins to poke itself over the edge of the step edge, it feels a stronger energetic driving force from the proximal exposed C atoms and the less steep step edge that encourages the sexiphenyl molecule (with its greater rotational freedom) to bend round the step and pick up the energy advantage of the π-π interactions. This example of an

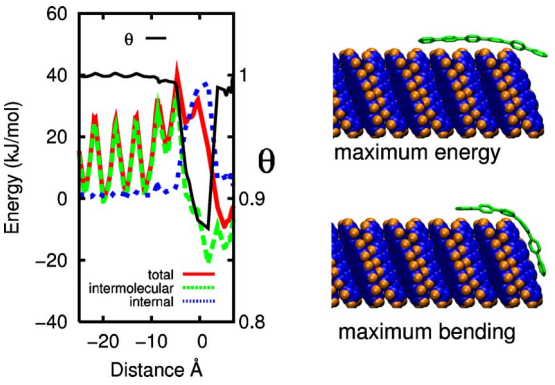

FIG. 21. (Color online) The energetic profile (left) and key snapshots (right) of an orthogonal trajectory of a sexiphenyl molecule (not the minimum-energy path) as it descends over a DIP step edge in which the sexiphenyl molecule gradually bends over the step edge. Note the spikes in energy as the uncomfortably oriented molecule traverses the terrace and the relatively large period of energy loss during the descent.

eventuality in which descending molecules can continuously drape themselves over steps) illustrates the kinds of molecules (orientationally more free molecules) and step edges (less steep, π cloud exposed) that are more likely to give rise to heavily bent descents.

APPENDIX C: LARGER-SCALE SIMULATIONS—PENTACENE

In the main article, all of the step-edge molecules and atoms were frozen in place as predicted by the MM3π potential. Then, during subsequent calculations, the MM3 potential was used to describe the step-edge molecules while the MM3π potential was used solely for the descending molecule. This was required as the MM3π potential becomes very computationally expensive when used on large numbers of atoms (on the order of hundreds). To carry out dynamic simulations or geometry optimizations where the molecules and atoms comprising the step edge are free to move, in addition to the descending molecule, requires that an accurate but computationally efficient potential be employed to describe the now liberated step-edge molecules. We have shown that, unless the MM3π model is used for π-conjugated molecules, an incorrect planar molecular structure of certain molecules is predicted, specifically rubrene and sexiphenyl. We cannot use the MM3π potential for the entire system (descending molecule+step edge) due to computational expense and therefore employ a system where the MM3 potential can be used with as much confidence with or without the MP2 correction. For the five fused-ring molecules that we considered (the acenes, DIP, and C60), the correct molecular structure is observed without the MP2 correction, but a smaller C=C bond length is observed ($\approx$0.05 Å smaller, depending on the locality). For pentacene, this results in a molecule which is 13.61 Å in length instead of 14.14 Å but the intermolecular energy is largely unaffected. In previous work[70] we have established the ability of the MM3 potential to describe the interactions within the herringbone crystal structure in dynamic simulations of a similar system and for this reason we chose pentacene as the system for our larger scale and dynamic simulations. As an additional justification of the utilization of the MM3 potential in place of the MM3π potential we also carried out the following calculations for the pentacene system.

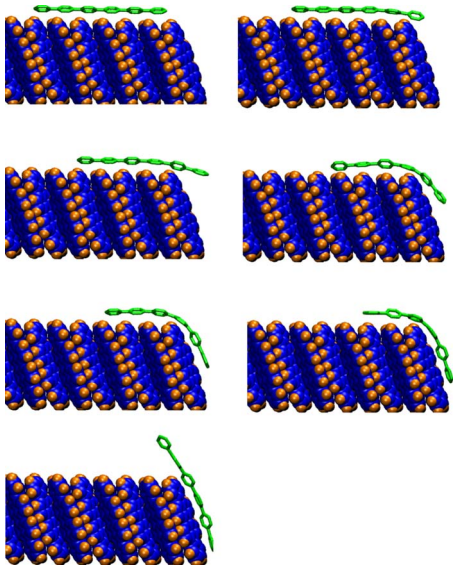

FIG. 22. (Color online) More detailed snapshots of the orthogonal trajectory from Fig. 21.

The entire procedure, to quantify the self-Schwöebel barrier for pentacene was repeated with different sets of restrictions placed on the system so as to decouple the effects of choice of model and the disposition of the molecules forming the step-edge (frozen in place and unable to move in response to the presence of the descending molecule, or not). The cases we considered were: (1) original case—All molecules forming the step-edge frozen in place. MM3π model used to describe the descending molecule. (2) All step molecules frozen. The MM3 model used for the descending molecule. (3) All step molecules free to move. The MM3π model used for the descending molecule. (4) All step molecules free to move. The MM3 model used for the descending molecule.

We show, in Fig. 23, the minimum trajectories resulting from the four different cases: all of the trajectories, transition points, and barriers are very similar. A horizontal comparison of the graphs indicates that the use of the MM3π potential for the descending molecule is unnecessary, for a comparable level of accuracy is achieved when the MM3 potential is employed for the descending molecule for both frozen and unfrozen step edges. When the molecules constituting the step are free to move, we see no mechanism by which the molecules substantially affect (either to assist or hinder) the descent of the molecule and the resulting step-edge barrier is only 5 kJ/mol lower when all the molecules are free to move and accommodate the descending molecule. The molecules in the step do not move significantly when the descending molecule passes by in close proximity and retain positions close to those originally described by the MM3π potential.

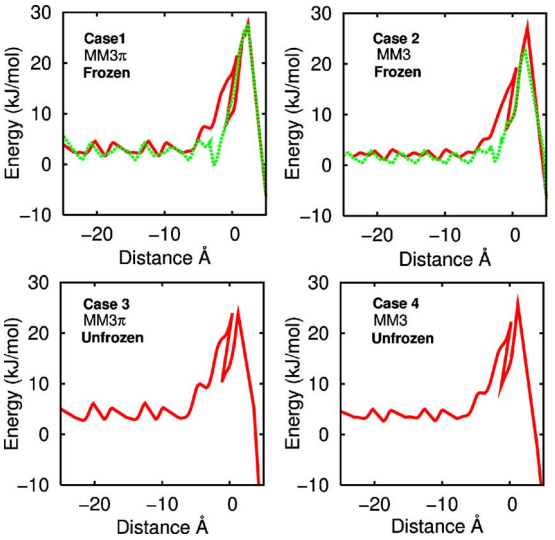

FIG. 23. (Color online) A comparison of the minimum-energy Schwöebel barriers for the four test cases of constraint. For each graph, the label Frozen or "Unfrozen" refers to the disposition of the step-edge molecules and the labels MM3 and MM3π refer to the potential model used to describe the intermolecular interactions of the descending molecule.

Pentacene: Dynamics of step-edge descent

To investigate how the step-edge barrier was affected by thermal movement of the molecules or atoms, we performed molecular-dynamic simulations of the pentacene system. In this way, we could study not only the minimum energy path but observe the interplay of kinetic and thermodynamic aspects of step-edge descent.

All of the molecular-dynamics simulations were carried out using the MM3 potential applied to all molecules in the system. The construction of a more complex step edge with two layers was also required; the bottom layer frozen and the top layer was free to move. The top layer was thermalized to a temperature of 300 K for 40 ps in a constant-temperature simulation (NVT ensemble) to allow it to come to a quasi-equilibrium condition and then a single diffusing molecule on the upper surface was directed orthogonally toward the step edge from a series of random starting points and orientations.

Because the step-edge barrier is significant compared to the thermal energy of the molecule, we cannot simply rely on the molecule to make a successful attempt to descend the step edge of its own accord during the limited period of observation (order of nanoseconds) of the MD simulation. When the initial location of the molecule was constrained to lie within 5 Å of the step and a constant-temperature, NVT, simulation was run at 300 K for longer time scales (i.e., 10s of ns), the molecule free to diffuse over the terrace was not observed to fall down the step once. Assuming a Boltzmann relationship defined by an attempt frequency, ν_0, and an activation energy, ΔE_{ES}, given in the equation below, the molecule would need to approach the step edge 2300 times for every successful descent. This estimate of the probability of observing a spontaneous descent was larger than the number of trials in our study.

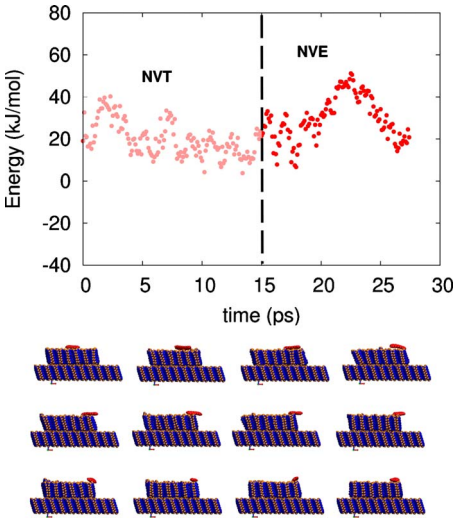

FIG. 24. (Color online) Time trajectory of a failed dynamic step-edge descent followed using molecular-dynamics molecular simulations. The graph shows the intermolecular energy between the molecule and the step as a function of time. Before 15 ps, the system is held at thermal equilibration under constant-temperature, NVT, conditions. At 15 ps, the molecule is directed toward the step edge with the aid of a harmonic potential placed on the middle phenyl ring. The energy of the system rises by about 10 kJ/mol as the molecule experience the step-edge barrier at about 22 ps. The snapshots shown below the energy-time plot are taken looking down the b axis at 1 ps intervals from 16–27 ps and the molecules are color coded to correspond with the graph.

$$\nu = \nu_0 e^{-(\Delta E_{ES}/k_B T)}. \tag{C1}$$

To finesse this problem, the diffusing molecule on the upper terrace was directed across the surface by imposing a harmonic potential on the central phenyl ring until it was within 10 Å of the step edge. At this point, the potential was then lifted and the system evolved under a microcanonical, constant-energy, NVE ensemble. At each random starting position (varying both rotational and translational initial conditions), eight simulations were carried out with varying force constants, thus varying the energy of approach to the step edge. The lowest-energy successful trajectories and highest-energy unsuccessful trajectories were then analyzed. All of the trajectories in Figs. 24–26 use the intermolecular energy between the descending molecule and the step edge on the ordinate axis. The internal energy of the molecule remains roughly constant and we see very little deformation in the step edge as the molecule approaches.

Figure 24 shows one of the many failed trajectories where the molecule approaches the step edge only to be repelled back away from it. The loss in binding energy is at least equivalent to that of the successful descents shown in Fig. 25, indicating the importance of the molecule's approach in considering the likelihood of a successful descent. The two trajectories shown in Fig. 25 are both successful descents; the red molecule (top trajectory) descends in a more orthogonal orientation with a slightly higher loss in binding energy than the parallel green molecule, though the difference is marginal. We are not claiming that these successful descents represent the global lowest-energy descents because of the

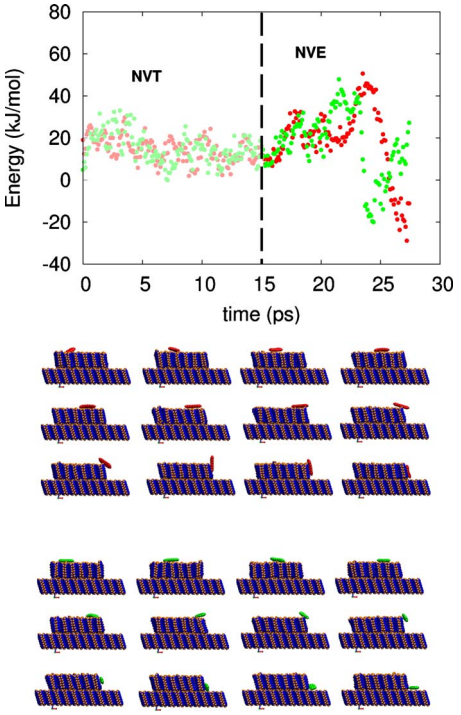

FIG. 25. (Color online) Two molecular-dynamics simulation trajectories of two successful dynamic step-edge descents (one shown in red, the other in green, on the energy-time plot on the upper part of the figure). The energy rise at the step edge is clearly larger than in the preceding figure (of over 20 kJ/mol) but, like the preceding figure, the maximum energy occurs at the tipping point (around 22–24 ps). The key is the same as that given in the caption for Fig. 24.

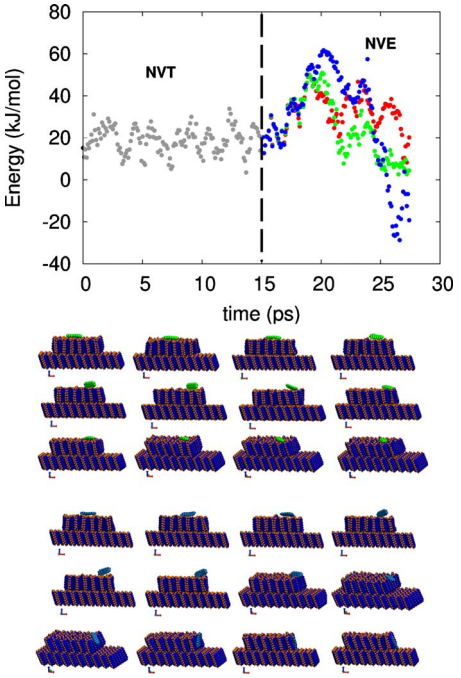

FIG. 26. (Color online) Three trajectories, all starting from the same position but with different initial energies (red being the lowest in energy, followed by green, and then blue). The key is the same as in Fig. 24 with the exception that the NVT portion trajectory is shown in gray. Snapshots of the red trajectory are not shown. Here again, the unsuccessful descents of the red and green molecules are seen not to experience a high-enough energy rise to overcome the Schwöebel barrier whereas the energy-time profile of the blue trajectory is able to do so and fall over the step edge.

imposed directional bias that we place on the dynamic simulations. And, indeed, the loss in binding energy is higher than we observed in our static energy minimizations. In order to claim that we have observed the dynamics of such a global energy situation, we would need to sample the true diffusional paths available to the molecule; by biasing the progress of the molecule toward the step edge, this is compromised.

In Fig. 26, we demonstrate the difficulty of overcoming the step-edge energy barrier in dynamic simulations: All three molecular trajectories shown on the top graph (red, green, and blue) start at the same position but are accelerated toward the step edge with slightly different energies (ascending in energy from red to green to blue). All three trajectories become unstable around 18–19 ps and the molecule leaves the (001) surface briefly (by rotating onto its edge, rather than lying flat on the surface), resulting in a loss in binding energy with the surface. In the cases denoted in red and green, the molecule falls back flat onto the step edge at a time stamp of 22 ps but still fails to fall off the edge. This is because, in both cases, the molecule hits the last row of molecules in the step edge. In the case of the "blue" molecule, its slightly higher energy allows it the momentum to just clear the surface, enabling it to fall over the edge. Importantly, in all three cases, despite the high energies involved, the step edge maintains its structural integrity throughout. This provides further justification for the assumption that the molecules in the step edge are largely passive in any Schwöebel barrier descent mechanism and that the degrees of freedom of molecules in the step edge can be frozen out.

*pqc1@cornell.edu

[1] R. L. Schwoebel and E. J. Shipsey, J. Appl. Phys. **37**, 3682 (1966).
[2] G. Ehrlich and F. G. Hudda, J. Chem. Phys. **44**, 1039 (1966).
[3] S. K. Xiang and H. Huang, Appl. Phys. Lett. **92**, 101923 (2008).
[4] A. Bogicevic, J. Strömquist, and B. I. Lundqvist, Phys. Rev. Lett. **81**, 637 (1998).
[5] R. Stumpf and M. Scheffler, Phys. Rev. B **53**, 4958 (1996).
[6] S. Kodiyalam, K. E. Khor, and S. Das Sarma, Phys. Rev. B **53**, 9913 (1996).
[7] M. Fendrich and J. Krug, Phys. Rev. B **76**, 121302(R) (2007).
[8] G. Hlawacek, P. Puschnig, P. Frank, A. Winkler, C. Ambrosch-Draxl, and C. Teichert, Science **321**, 108 (2008).
[9] R. Cantrell and P. Clancy, Surf. Sci. **602**, 3499 (2008).

[10] *Organic Field-Effect Transistors*, Optical Science and Engineering, edited by Z. Bao and J. Locklin (CRC, Boca Raton, 2007).
[11] *Organic Electronics: Materials, Manufacturing, and Applications (Hardcover)*, edited by H. Klauk (Wiley-VCH, Weinheim, 2006).
[12] S. R. Forrest, Nature (London) **428**, 911 (2004).
[13] J. C. Tai and N. L. Allinger, J. Comput. Chem. **19**, 475 (1998).
[14] N. L. Allinger, Y. H. Yuh, and J. H. Lii, J. Am. Chem. Soc. **111**, 8551 (1989).
[15] J. H. Lii and N. L. Allinger, J. Am. Chem. Soc. **111**, 8566 (1989).
[16] J. H. Lii and N. L. Allinger, J. Am. Chem. Soc. **111**, 8576 (1989).
[17] S. J. Stuart, A. B. Tutein, and J. A. Harrison, J. Chem. Phys. **112**, 6472 (2000).
[18] The TORSION term is an explicit four-body potential that describes various dihedral angle preferences in hydrocarbon configurations.
[19] M. J. Frisch *et al.*, GAUSSIAN03, Revision C.02, Gaussian, Inc., Wallingford, CT, 2004.
[20] S. Plimpton, J. Comput. Phys. **117**, 1 (1995).
[21] S. Plimpton, R. Pollock, and M. Stevens, in Proceedings of the Eighth SIAM Conference on Parallel Processing for Scientific Computing, Minneapolis, MN, 1997 (unpublished).
[22] J. W. Ponder, TINKER—software tools for molecular design (2004).
[23] P. Puschnig, D. Nabok, and C. Ambrosch-Draxl, in *Interface Controlled Organic Thin Films*, Springer Proceedings in Physics, edited by H. G. Rubahn, H. Sitter, G. Horowitz, and K. Al-Shamery (SPVB, Berlin, Heidelberg, 2009), p. 3.
[24] S. Guha, W. Graupner, R. Resel, M. Chandrasekhar, H. R. Chandrasekhar, R. Glaser, and G. Leising, Phys. Rev. Lett. **82**, 3625 (1999).
[25] L. Claes, J. P. Francois, and M. S. Deleuze, Chem. Phys. Lett. **339**, 216 (2001).
[26] A. S. Paraskar, A. R. Reddy, A. Patra, Y. H. Wijsboom, O. Gidron, L. J. W. Shimon, G. Leitus, and M. Bendikov, Chem.-Eur. J. **14**, 10639 (2008).
[27] M. P. Johansson and J. Olsen, J. Chem. Theory Comput. **4**, 1460 (2008).
[28] J. C. Sancho-García and J. Cornil, J. Chem. Theory Comput. **1**, 581 (2005).
[29] F. Grein, Theor. Chem. Acc. **109**, 274 (2003).
[30] S. Tsuzuki, T. Uchimaru, K. Matsumura, M. Mikami, and K. Tanabe, J. Chem. Phys. **110**, 2858 (1999).
[31] E. Fabiano and F. D. Sala, Chem. Phys. Lett. **418**, 496 (2006).
[32] F. Grein, J. Mol. Struct. THEOCHEM **624**, 23 (2003).
[33] S. Mayo, B. Olafson, and W. Goddard, J. Phys. Chem. **94**, 8897 (1990).
[34] S. Verlaak, S. Steudel, P. Heremans, D. Janssen, and M. S. Deleuze, Phys. Rev. B **68**, 195409 (2003).
[35] C. C. Mattheus, G. A. de Wijs, R. A. de Groot, and T. T. M. Palstra, J. Am. Chem. Soc. **125**, 6323 (2003).
[36] R. G. D. Valle, A. Brillante, E. Venuti, L. Farina, A. Girlando, and M. Masino, Org. Electron. **5**, 1 (2004).
[37] T. Arikawa, N. Tajima, S. Tsuzuki, K. Tanabe, and T. Hirano, J. Mol. Struct. THEOCHEM **339**, 115 (1995).
[38] R. Resel, Proceedings from the 12th International Conference on Thin Films [Thin Solid Films **433**, 1 (2003)].
[39] These minimum energy trajectories are for the step-edge sexiphenyl-β as described in the supplemental appendix.
[40] H. H. Fong, S. K. So, W. Y. Sham, C. F. Lo, Y. S. Wu, and C. H. Chen, Chem. Phys. **298**, 119 (2004).
[41] O. D. Jurchescu, A. Meetsma, and T. T. M. Palstra, Acta Crystallogr., Sect. B: Struct. Sci. **62**, 330 (2006).
[42] B. Chapman, A. Checco, R. Pindak, T. Siegrist, and C. Kloc, J. Cryst. Growth **290**, 479 (2006).
[43] R. B. Campbell, J. M. Robertson, and J. Trotter, Acta Crystallogr. **14**, 705 (1961).
[44] R. B. Campbell, J. M. Robertson, and J. Trotter, Acta Crystallogr. **15**, 289 (1962).
[45] A. C. Dürr *et al.*, Phys. Rev. B **68**, 115428 (2003).
[46] R. Mason, Acta Crystallogr. **17**, 547 (1964).
[47] P. A. Heiney, J. E. Fischer, A. R. McGhie, W. J. Romanow, A. M. Denenstein, J. P. McCauley, Jr., A. B. Smith, and D. E. Cox, Phys. Rev. Lett. **66**, 2911 (1991).
[48] C. C. Mattheus, A. B. Dros, J. Baas, G. T. Oostergetel, A. Meetsma, J. L. de Boer, and T. T. M. Palstra, Synth. Met. **138**, 475 (2003).
[49] T. Siegrist, C. Besnard, S. Haas, M. Schiltz, P. Pattison, D. Chernyshov, B. Batlogg, and C. Kloc, Adv. Mater. **19**, 2079 (2007).
[50] A. C. Dürr, F. Schreiber, M. Münch, N. Karl, B. Krause, V. Kruppa, and H. Dosch, Appl. Phys. Lett. **81**, 2276 (2002).
[51] J. E. Northrup, M. L. Tiago, and S. G. Louie, Phys. Rev. B **66**, 121404(R) (2002).
[52] D. Nabok, P. Puschnig, and C. Ambrosch-Draxl, Phys. Rev. B **77**, 245316 (2008).
[53] J. H. Seo *et al.*, Appl. Phys. Lett. **89**, 163505 (2006).
[54] M. Haemori, J. Yamaguchi, S. Yaginuma, K. Itaka, and H. Koinuma, Jpn. J. Appl. Phys., Part 1 **44**, 3740 (2005).
[55] H. Liu, Z. Lin, L. V. Zhigilei, and P. Reinke, J. Phys. Chem. C **112**, 4687 (2008).
[56] P. Sullivan and T. Jones, Org. Electron. **9**, 656 (2008).
[57] A. M. C. Ng, A. B. Djurisic, W.-K. Chan, and J.-M. Nunzi, Chem. Phys. Lett. **474**, 141 (2009).
[58] S. Yoo *et al.*, Solid-State Electronics **51**, 1367 (2007), special issue on papers selected from the NGC2007 Conference.
[59] A. Amassian, V. A. Pozdin, T. V. Desai, S. Hong, A. R. Woll, J. D. Ferguson, J. D. Brock, G. G. Malliaras, and J. R. Engstrom, J. Mater. Chem. **19**, 5580 (2009).
[60] C. F. Matta, J. Hernández-Trujillo, and T.-H. Tang, Chemistry **9**, 1940 (2003).
[61] L. F. Pacios and L. Gómez, Chem. Phys. Lett. **432**, 414 (2006).
[62] O. Bastiansen and S. Samdal, J. Mol. Struct. **128**, 115 (1985).
[63] A. Almenningen, O. Bastiansen, L. Fernholt, B. N. Cyvin, S. J. Cyvin, and S. Samdal, J. Mol. Struct. **128**, 59 (1985).
[64] E. P. Socci, B. L. Farmer, and W. W. Adams, J. Polym. Sci., Part B: Polym. Phys. **31**, 1975 (1993).
[65] K. N. Baker, A. V. Fratini, T. Resch, H. C. Knachel, W. Adams, E. Socci, and B. Farmer, Polymer **34**, 1571 (1993).
[66] V. Lukeš, R. Šolc, M. Barbatti, M. Elstner, H. Lischka, and H.-F. Kauffmann, J. Chem. Phys. **129**, 164905 (2008).
[67] C. Ambrosch-Draxl, J. A. Majewski, P. Vogl, and G. Leising, Phys. Rev. B **51**, 9668 (1995).
[68] K. Saito, Y. Yamamura, and M. Sorai, Bull. Chem. Soc. Jpn. **73**, 2713 (2000).
[69] R. Resel, J. Phys.: Condens. Matter **20**, 184009 (2008).
[70] J. Goose and P. Clancy, J. Phys. Chem. C **111**, 15653 (2007).